Single-Cell Transcriptional Signatures of Glomerular Disease in Transgenic Mice with APOL1 Variants

Teruhiko Yoshida[1], *Khun Zaw Latt*[1], *Briana A. Santo*[2], *Shashi Shrivastav*[1], *Yongmei Zhao*[3], *Paride Fenaroli*[4,5], *Joon-Yong Chung*[6], *Stephen M. Hewitt*[6], *Vincent M. Tutino*[2], *Pinaki Sarder*[2,7], *Avi Z. Rosenberg*[4], *Cheryl A. Winkler*[3], *and Jeffrey B. Kopp*[1]

Key Points

- Apolipoprotein L1 (APOL1)-G1 induced kidney disease in the two APOL1 transgenic mouse models, HIV-associated nephropathy and IFN-γ administration.
- Glomerular single-nuclear RNA-sequencing identified genes differentially expressed among mice with APOL1-G1 and G0 variants at single-cell resolution.

Abstract

Background Apolipoprotein L1 (*APOL1*) high-risk variants contribute to kidney disease among individuals with African ancestry. We sought to describe cell-specific APOL1 variant–induced pathways using two mouse models.

Methods We characterized bacterial artificial chromosome/APOL1 transgenic mice crossed with HIV-associated nephropathy (HIVAN) Tg26 mice and bacterial artificial chromosome/APOL1 transgenic mice given IFN-γ.

Results Both mouse models showed more severe glomerular disease in APOL1-G1 compared with APOL1-G0 mice. Synergistic podocyte-damaging pathways activated by APOL1-G1 and by the HIV transgene were identified by glomerular bulk RNA sequencing (RNA-seq) of HIVAN model. Single-nuclear RNA-seq revealed podocyte-specific patterns of differentially expressed genes as a function of *APOL1* alleles. Shared activated pathways, for example, mammalian target of rapamycin, and differentially expressed genes, for example, *Ccn2*, in podocytes in both models suggest novel markers of APOL1-associated kidney disease. HIVAN mouse-model podocyte single-nuclear RNA-seq data showed similarity to human focal segmental glomerulosclerosis glomerular RNA-seq data. Differential effects of the *APOL1*-G1 variant on the eukaryotic initiation factor 2 pathway highlighted differences between the two models.

Conclusions These findings in two mouse models demonstrated both shared and distinct cell type–specific transcriptomic signatures induced by APOL1 variants. These findings suggest novel therapeutic opportunities for APOL1 glomerulopathies.

JASN 35: 1058–1075, 2024. doi: https://doi.org/10.1681/ASN.0000000000000370

Introduction

Apolipoprotein L1 (*APOL1*) high-risk variants discovered in 2010[1,2] explain a substantial proportion of the high prevalence of kidney diseases in individuals with sub-Saharan African ancestry.[3] Carriage of two *APOL1* high-risk variants accounts for much of the excess risk of kidney failure, FSGS, and HIV-associated nephropathy (HIVAN) among Black individuals, 12%–14% of whom carry high-risk genotypes.[4] The utility of *APOL1* genotype testing is under consideration in various clinical settings, and APOL1 inhibition is under investigation in clinical trials.[5–7]

The molecular mechanisms by which *APOL1* high-risk variants damage glomerular cells remain incompletely understood. While many mechanisms have been reported in cell culture models, few have been demonstrated to be active in transgenic mouse models.[3,8] APOL1 is believed to cause podocyte damage primarily by intracellular expression, as reported in podocyte-specific overexpression mouse models.[9,10] APOL1 disease mechanisms have been

[1]Kidney Disease Section, Kidney Diseases Branch, NIDDK, NIH, Bethesda, Maryland
[2]Department of Pathology and Anatomical Sciences, Jacobs School of Medicine & Biomedical Sciences, University at Buffalo, Buffalo, New York
[3]Frederick National Laboratory for Cancer Research, NCI, NIH, Frederick, Maryland
[4]Department of Pathology, Johns Hopkins Medical Institutions, Baltimore, Maryland
[5]S.C. Nefrologia e Dialisi, AUSL-IRCCS, Reggio Emilia, Italy
[6]Center for Cancer Research, NCI, NIH, Bethesda, Maryland
[7]College of Medicine, University of Florida, Gainesville, Florida

Correspondence: Dr. Teruhiko Yoshida, email: yoshidateruhiko@g.ecc.u-tokyo.ac.jp

Received: December 21, 2023 **Accepted:** April 26, 2024
Published Online Ahead of Print: May 6, 2024

investigated using several animal models, including the bacterial artificial chromosome (BAC)/APOL1 transgenic mouse model, which mimics human *APOL1* expression regulated by the human *APOL1* promotor and other regulatory elements.[11–16] Of the many APOL1-associated kidney diseases, HIVAN has the strongest association with *APOL1* high-risk genotypes, with odds ratios of 29 and 89 in the United States and South Africa, respectively.[17,18]

In this study, we describe molecular pathways using perhaps the most relevant translational mouse model of APOL1 expression, BAC/APOL1 mice; these mice were crossed with HIVAN (Tg26) mice.[19,20] We also induced acute glomerular injury by administering IFN-γ to BAC/APOL1 mice to drive increased APOL1 expression.

These experiments allowed us to address the hypothesis that APOL1 variant–driven cell-specific injury pathways are shared between the two models. We also examined APOL1 variant–related RNA sequencing (RNA-seq) data from patients with FSGS in the Nephrotic Syndrome Study Network (NEPTUNE).

Methods

Mice

Mouse experiments were conducted in accordance with the National Institutes of Health (NIH) Guide for the Care and Use of Laboratory Animals and were approved in advance by the National Institute of Diabetes and Digestive and Kidney Diseases Animal Care and Use Committee (Animal study proposal, K097-KDB-17 and K096-KDB-20). We studied both male and female mice. Mice were housed in cages on a constant 12-hour light/dark cycle, with controlled temperature and humidity and food and water provided *ad libitum*. Sample sizes for experiments were determined without formal power calculations. Mice with large cutaneous papilloma were excluded. Investigators were not masked to group allocation, but were masked when assessing outcomes.

We used human *APOL1* gene locus transgenic mice (BAC/APOL1 mice),[13,14] generated using a BAC-containing APOL1-G0 or variant G1 allele. As previously described, an approximately 47 kb human DNA fragment, encompassing only the human *APOL1* gene with 5′ and 3′ flanking regions (including exons 1 and 2 of *APOL2* and 3′ region including exons 39–41 of part of *MYH9* gene), was isolated and subcloned from human BAC clone (ENST00000397278, which corresponds to NM_003661). These BAC subclones include APOL1 amino acid sequence of E150, M228, and R255.[21] Individual APOL1-G0 and G1 BAC subclones were injected into 129SvJ/B6N F1 mouse embryos, and the founder mice were subsequently backcrossed onto the 129SvJ background.

For the HIVAN model mouse, we bred hemizygous BAC/APOL1-G0/G1 mice with Tg26 mice to obtain F1 generation of BAC/APOL1xTg26 dual transgenic mice to be used for experiments. We measured both weights and collected random urine samples at 6 and 9 weeks of age. We used 9-week-old mice for phenotype characterizations, including glomerular extraction and collection of kidneys and blood as described below.

For IFN-γ model experiments, we injected a single dose of recombinant murine IFN-γ (CYT-358, ProSpec, East Brunswick, NJ) in PBS at 1.125×10^7 U/kg body weight, retro-orbitally under isoflurane anesthesia (0 hour).[16] Urine was collected every 24 hours using metabolic cages, beginning 24 hours before IFN injection and ending 72 hours after injection. Selected mice were euthanized at 24 hours for further experiments.

Urinary Albumin and Creatinine Measurement

We determined the urinary albumin levels with Albuwell M (Mouse Albumin ELISA) (1011, Ethos Biosciences, Logan Township, NJ). We measured urine creatinine concentrations with the Creatinine Companion kit (1012, Ethos Biosciences). Albuminuria was determined as the ratio of urinary albumin to creatinine. All procedures were performed in accordance with the manufacturers' protocols.

In Situ Hybridization

Mouse kidney tissues were fixed with 10% buffered formalin for 24 hours and embedded in paraffin. Chromogenic *in situ* detection was performed on tissue sections from the mouse formalin-fixed paraffin-embedded (FFPE) blocks using the RNAscope *in situ* hybridization (ISH) (Advanced Cell Diagnostics, Bio-Techne, Minneapolis, MN). In brief, 5-μm FFPE tissue sections were deparaffinized, boiled with RNAscope Target Retrieval Reagent for 15 minutes at 99°C, and protease digested at 40°C for 30 minutes. This was followed by hybridization for 2 hours at 40°C with probe-Hs-APOL1-O1 (439871, Advanced Cell Diagnostics). In addition, Probe-Mm-PPIB (313911) and Probe-DapB (310043) were used for positive and negative control, respectively. Probes were detected with a RNAscope 2.5 HD Reagent Kit (Brown) (322310).

Fluorescent *in situ* detection of mRNA was performed using RNA probe-Hs-APOL1-No-XMm (459791), Mm-Nphs1 (433571), Nell2 (1093741), St6galnac3 (1170041), and Ccn2 (1170051). Specific probe binding sites were visualized using an RNAscope Hiplex12 Reagents Kit (488, 550, 650) v2 (Advanced Cell Diagnostics, Bio-Techne) (324419). A Nikon Sora microscope in the National Institute of Diabetes and Digestive and Kidney Diseases Advanced Light Microscopy Imaging Analysis Core facility was used for fluorescence imaging.

Immunohistochemistry and Immunofluorescence Staining

FFPE tissue sections were deparaffinized and rehydrated. Antigen retrieval was performed by heating in citrate-buffered medium for 15 minutes in a 99°C hot water bath. Tissues were blocked by 2.5% normal horse serum. Sections were incubated for 1 hour at room temperature with primary antibodies against ribosomal protein S6 (2217, Cell Signaling, 1:100 dilution), phospho-ribosomal protein S6 (Ser240/244) (5364, Cell Signaling, 1:1000 dilution), phospho-4E-BP1 (Thr37/46) (2855, Cell Signaling, 1:800 dilution), podocalyxin (AF1556, Bio-Techne, 5 μg/ml), and APOL1 (5.17D12, rabbit monoclonal, Genentech [South San Francisco, CA], 5 μg/ml).[22] Sections were processed following the ImmPRESS horseradish peroxidase (HRP) Universal Antibody (horse anti-mouse/rabbit IgG) Polymer Detection Kit and ImmPACT 3,3′-diaminobenzidine EqV Peroxidase (HRP) Substrate (Vector Laboratories, Burlingame, CA) protocol and counterstained with hematoxylin for chromogenic

detection. Sections were incubated for 1 hour with secondary antibodies with fluorophores for fluorescence detection.

Mouse kidney tissues were harvested and embedded in an optimal cutting temperature compound and frozen. Frozen blocks were sectioned at 5 μm. Sections were hydrated in PBS and blocked with 10% BSA/PBS for 1 hour in a humidified chamber. Alexa Fluor 647 anti-mouse F4/80 Antibody (123121, BioLegend, San Diego, CA, 1:25 dilution) was applied and incubated overnight at 4°C. After 4′,6-diamidino-2-phenylindole nuclear staining and mounting, slides were imaged by fluorescence microscopy.

Confocal Microscopy

A Yokogawa CSU-W1 SoRa spinning disk confocal scan head (Yokogawa, Sugar Land, TX), with a 50-μm pinhole (standard confocal mode, without SoRa imaging), mounted on a Nikon Ti2 microscope running NIS-elements 5.21.02 software (Nikon Instruments, Melville, NY), was used to collect tiles of multicolor fluorescence images. Fluorescence image channels were obtained sequentially, while sharing the Yokogawa T405/488/568/647 dichroic beam splitter. For 4′,6-diamidino-2-phenylindole fluorescence, excited by the 405 nm laser, emission was filtered by ET455/58 (Chroma, Technology Corp, Bellows Falls, VT). Green fluorescence was excited by the 488-nm laser and emission filtered by ET520/40 (Chroma). Orange fluorescence was excited by the 561-nm laser and emission filtered by ET605/52 (Chroma). Far red fluorescence was excited by the 640-nm laser and emission filtered by ET655LP (Chroma). Images were acquired with the Nikon Apo total internal reflection fluorescence 60×/1.49 Oil differential interference contrast N2 objective lens, producing a confocal section thickness of 1.2 μm for all fluorescence channels.

Transmission Electron Microscopy and Foot Process Effacement Evaluation

Mouse kidney sections, approximately 1 mm^3, were fixed for 48 hours at 4°C in 2.5% glutaraldehyde and 1% paraformaldehyde in 0.1 M cacodylate buffer (pH 7.4) and washed with cacodylate buffer three times. Tissues were fixed with 1% OsO_4 for 2 hours, washed again with 0.1 M cacodylate buffer three times, washed with water, and placed in 1% uranyl acetate for 1 hour. Tissues were serially dehydrated in ethanol and propylene oxide and embedded in EMBed 812 resin (Electron Microscopy Sciences, Hatfield, PA). Thin sections (approximately 80 nm) were obtained with a Leica Ultracut-UCT ultramicrotome (Leica, Deerfield, IL), placed onto 300 mesh copper grids and stained with saturated uranyl acetate in 50% methanol, followed by lead citrate. Grids were viewed with a JEM-1200EXII electron microscope (JEOL Ltd., Tokyo, Japan) at 80 kV, and images were recorded on the XR611M, mid-mounted, 10.5 M pixel, charge coupled devices camera (Advanced Microscopy Techniques Corp, Danvers, MA). We evaluated for foot processes effacement by filtering the surface of open capillary loops, using an image processing software (ImageJ, Viewpoint Light). We measured the length of the outer surface of the glomerular basal membrane. Overlying foot processes were counted by hand. A ratio of foot process number to glomerular basement membrane (GBM) length was computed for each image.

Mouse Kidney Pathological Evaluation

FFPE mouse kidney tissue sections, cut at 4 μm, were stained with hematoxylin and eosin, periodic acid–Schiff (PAS) reagents for routine and quantitative histological assessment.

Estimation of Glomerular Podocyte Count

"PodoCount,"[23] a computational tool for whole slide podocyte number estimation from digitized histologic sections, was used to detect, enumerate, and characterize podocyte nuclear profiles in the glomeruli of immunohistochemically labeled mouse kidney sections. FFPE tissues (2 μm thickness) were immunostained for $p57^{kip2}$, a marker of podocyte terminal differentiation (ab75974, Abcam, Cambridge, United Kingdom), and detected with horseradish peroxidase (RU-HRP1000, Diagnostic BioSystems, Pleasanton, CA) and diaminobenzidine chromogen substrate (BSB0018A, Bio SB, Santa Barbara, CA). PAS post-stain was applied without hematoxylin counterstain. PodoCount uses a combination of structural segmentation steps that use thresholding, a convolutional neural network,[24] and stain deconvolution; morphological image processing approaches to refine segmentation; and literature-informed feature engineering steps to compute various histologic podometrics[25] with correction for section thickness.[26] In this study, PodoCount was used to assess mean glomerular podocyte count and podocyte density per mouse.

Glomerular Isolation

Mice were anesthetized with 2, 2, 2-trimbromoethanol (Avertin, Sigma-Aldrich, St. Louis, MO), the abdominal aorta was exposed, and a cannula was inserted under a microscope into the aorta with a polyethylene-10 tube attached to a PE-50 tube. After clipping the celiac trunk, superior mesenteric artery, and aorta proximal to renal arteries, kidneys were perfused with PBS through the cannula. A small incision was made in the proximal left renal vein to assure good reagent perfusion, and a clip was placed on the left kidney vessels. The right kidney was perfused twice with PBS, containing 10 μl of Dynabeads M-450 tosylactivated (14013, Invitrogen, Waltham, MA). The right kidney was extracted for glomerular isolation, and the left kidney was extracted for pathological characterization.

The right kidney was placed in HBSS on ice. The kidney was minced with razor blades. Kidney fragments were placed in a solution containing 4 mg/ml of collagenase A (10103586001, Roche, Mannheim, Germany) and 200 units/ml of DNase I (04716728001, Roche) for 30 mins at 37°C with 1500 rpm agitation. A 100-μm strainer (542000, Greiner Bio-One, Frickenhausen, Germany) and Dynal (ThermoFisher, Waltham, MA) magnet were used to isolate glomeruli, which were washed three times with PBS. For bulk RNA-seq samples, 500-μl QIAzol (QIAGEN, Hilden, Germany) was added to a 1.5-ml tube containing glomeruli from 1/6 of each kidney. For single-nuclear RNA-seq samples, purified glomeruli were snap frozen in 1.5-ml tubes.

Reverse Transcription-Quantitative PCR

Total RNA was extracted using an RNeasy Plus Universal Kit (73404, QIAGEN) following the manufacturer's protocol, including removal of genomic DNA. RNA (1 μg) was reverse transcribed using the GoScript Reverse Transcription System (A5001, Promega, Madison, WI). cDNA was measured by quantitative PCR with FastStart Universal SYBR Green Master (Rox) (04913850001, Sigma-Aldrich) using QuantStudio 6 (ThermoFisher). Relative mRNA levels were quantified by the delta-delta CT method, using β-actin as an endogenous control. Primers used are summarized in Supplemental Table 1.

Bulk Glomerular RNA-Sequencing

Isolated glomerular tissues from mice of eight genotypes (wild type [WT], G0, G1, G2, Tg26, G0xTg26, G1xTg26, G2xTg26; n=5, 3, 4, 3, 5, 5, 5, 4, respectively) were homogenized in QIAzol. Total RNA was extracted using the RNeasy Plus Universal Kit (73404, QIAGEN) following the manufacturer's protocol, including removal of genomic DNA. cDNA libraries were prepared and sequenced at the Frederick National Laboratory for Cancer Research, NCI, Frederick, MD.

Samples were pooled and sequenced on NovaSeq6000 S1 flow cell using Illumina TruSeq Stranded mRNA Library Prep and paired-end sequencing with read length 101 bps (2×101 cycles). Samples had 47–67 million reads passing a quality filter; more than 92% of base calls had a quality score above Q30. Sample reads were trimmed to remove adapters and low-quality bases using Cutadapt v1.18. Trimmed reads were mapped to the reference genome (Mouse mm10) and to transcripts (Ensembl v96 annotation) using STAR aligner v2.7.0f. Gene expression quantification was performed using the RSEM v1.3.1 tool. Sequencing and mapping statistics of bulk glomerular RNA-seq are presented in Supplemental Table 2. Original data files and count tables have been deposited in Gene Expression Omnibus (GSE227234).

Bulk Glomerular RNA-Sequencing: Gene-Set Enrichment Analysis and Network Analysis

DESeq2[27] was used for differential expression analysis from raw count data. Normalized data were used for gene-set enrichment analysis (GSEA). GSEA v4.1.0[28,29] was used for pathway enrichment analysis. Weighted gene coexpression network analysis package[30] was used for network analysis, using normalized count data from APOL1-G0, G1, G0xTg26, and G1xTg26 samples by DESeq2, to identify modules differentially related to the *APOL1* genotype and the Tg26 transgene. Network building and visualization of genes in the saddlebrown module were conducted by NetworkAnalyst 3.0 (https://networkanalyst.ca/).[31] Intersection of lists was mapped on the Search Tool for the Retrieval of Interacting Genes/Proteins Interactome database (900 confidence score with experimental evidence) (https://string-db.org/).

Single-Nucleus RNA-Sequencing

Nuclei from five isolated glomeruli sample types (WT, G0xTg26, G1xTg26, G0+IFN-γ, G1+IFN-γ) were prepared.[32] Snap-frozen isolated glomeruli were lysed in EZlysis buffer (NUC101-1KT, Sigma-Aldrich) and homogenized 30 times using a loose Dounce homogenizer and five times in a tight pestle. After 5 minutes of incubation, the homogenate was passed through a 40-μm filter (43-50040, PluriSelect, El Cajon, CA) and centrifuged at 500×g at 4°C for 5 minutes. The pellet was washed with EZlysis buffer and again centrifuged at 500×g at 4°C for 5 minutes. Pellets were resuspended with Dulbecco's Phosphate-Buffered Saline with 1% FBS and passed through a 5-μm filter (43-50005, PluriSelect) to make final nuclei prep for loading on to a 10x Chromium Chip G (10x Genomics, Pleasanton, CA) to form gel beads in emulsion.

Single-nuclear isolation, RNA capture, cDNA preparation, and library preparation were performed following the manufacturer's protocol (Chromium Next GEM Single Cell 3′ Reagent Kit, v3.1 chemistry, 10x Genomics). Prepared cDNA libraries were sequenced at the Frederick National Laboratory for Cancer Research. All samples had sequencing yields of at least 183 million reads. Over 95.7% of bases in the barcode regions had Q30 or above, and at least 93.5% of bases in the RNA reads had Q30 or above. More than 95.5% of bases in the unique molecular identifiers had Q30 or above.

Analyses were performed with the Cell Ranger v6.1.2 software (10x Genomics) using the default parameters and with pre-mRNA analysis turned on. The reference was built from the mouse (mm10) reference genome, supplemented with HIV-1 viral sequences and human *APOL1* sequences. The sequencing and mapping statistics of single-nucleus RNA-seq are presented in Supplemental Table 3. Original data files and count tables have been deposited in Gene Expression Omnibus (GSE227235).

Single-Nucleus RNA-Sequencing Analysis

Removal of ambient RNA was conducted by SoupX (version 1.5.2),[33] following the default protocol using "autoEstCont" and "adjustCounts" functions. After removal of ambient RNA, integration of single-nucleus gene expression data was performed using Seurat (version 4.0.5) and SeuratData (version 0.2.2)[34] after filtering out nuclei with any of the following features: detected genes numbers <200 or >4000, total RNA count >15,000, or mitochondrial transcript percentage >20%. After filtering, 20,276 nuclei remained for downstream analysis.

Clustering of the combined data used the first 30 principal components at a resolution of 0.6 and identified 21 distinct cell clusters. Cell types were identified by expression levels of known marker genes (as listed in Results). After clusters from tubules, fibroblasts, and doublets were removed, there remained 16,030 nuclei in 12 clusters (Supplemental Figure 3A). Differential expression analysis was performed using the "Findmarkers" function in Seurat, using default parameters. Differentially expressed genes (DEGs) were identified for each paired comparison (HIVAN: G1xTg26 versus G0xTg26; and IFN-γ: G1+IFN-γ versus G0+IFN-γ), using a cutoff of adjusted $P < 0.05$. Pathway analysis was performed using QIAGEN ingenuity pathway analysis (IPA)[35] software, with DEG sets as inputs. Cell–cell interaction analysis was performed using CellChat (version 1.5.0),[36] with mouse protein–protein interactions loaded.

GSEA of Human Glomerular RNA-Seq Data by APOL1 Genotype, Using Custom Gene Sets Derived from the DEG Gene Sets

Normalized human glomerular RNA-seq data were obtained from the website APOL1 Portal (http://APOL1portal.org).[37] Original data were from NEPTUNE,[38] a biopsy-based cohort of patients with primary glomerular kidney diseases.

Patient inclusion criteria for the study included the following: a histologic diagnosis of FSGS, available glomerular RNA-seq data, known *APOL1* genotype, and Black ancestry or genotype-predicted African continental ancestry.[37] DEG sets were obtained from single-nucleus RNA-seq analysis and were converted to custom human gene lists. GSEA analysis was conducted by GSEA v4.1.0, comparing data from a *APOL1* high-risk patient (defined as those carrying two *APOL1* kidney risk alleles) (n=16) and data from a *APOL1* low-risk patient (defined as those carrying zero or one *APOL1* kidney risk alleles) (n=14).

Pathway Analysis to Compare Transcriptomes of APOL1-G1/G2 Podocytes versus APOL1-G0/G0 Podocytes

Single-cell RNA-seq of urinary podocytes from patients with FSGS[39] and bulk RNA-seq of podocytes *in vitro* (human urine-derived podocyte-like cell lines)[40] were reported previously. We reanalyzed these data to compare pathways between APOL1-G1/G2 podocytes and APOL1-G0/G0 podocytes. The original data were obtained from GSE176465[39] and GSE194337.[40] DEGs were identified by the comparison of RNA count data, APOL1-G1/G2 versus APOL1-G0/G0. DEG sets as input for IPA analysis were defined using cutoffs as follows: adjusted $P < 0.05$ for differentiated human urine-derived podocyte-like cells and $P < 0.05$ without multiple testing correction for urine podocytes from patients with FSGS. Pathway analysis was performed using QIAGEN IPA[35] software, using the three DEG sets as inputs.

Results

Accelerated Glomerular Injury in APOL1-G1xTg26 HIVAN Mice

We established a dual transgenic mouse model BAC/APOL1xTg26 to elucidate the effect of *APOL1* genotype in the context of HIVAN (Figure 1A). BAC/APOL1-G2 mice showed lower expression of APOL1 compared with BAC/APOL1-G0 and -G1 mice (data not shown). Therefore, we decided to focus on characterizing APOL1-G0 and -G1 mice. Plasma creatinine (Figure 1B) and albuminuria (Figure 1C) levels indicated that G1xTg26 mice had the most kidney parenchymal injury, the latter suggesting primary glomerular/podocyte damage. Histomorphology revealed greater glomerular damage in BAC/APOL1-G1xTg26 mice compared with other genotypes (Figure 1D). We confirmed APOL1 expression by ISH and immunohistochemistry (Supplemental Figure 1A), which showed APOL1 mRNA and protein expression primarily in podocytes and renal endothelial cells.

Podocyte depletion in G1xTg26 mice was identified by p57 staining, followed by podocyte estimation using "PodoCount"-derived podometric analysis on the basis of podocyte count and podocyte density (Figure 1, D–F). Electron microscopy showed more prominent podocyte foot process effacement in G1xTg26 mice compared with G0xTg26 mice (Figure 1, G and H). These data indicate enhanced glomerular injury, particularly podocyte injury, in the HIVAN model in an APOL1-G1–dependent manner. No overt kidney disease was observed in Tg26 mice or in G0xTg26 mice. This indicates that the HIVAN model is a suitable model to study transcriptional change occurring earlier in the disease course by APOL1-G1.

IFN-γ Model Induced Proteinuria in BAC/APOL1-G1 Mice

We next investigated the effect of APOL1 on glomerular cells in a second APOL1-mediated kidney disease model, using the IFN-γ IV model (Figure 1I).[16] Compared with APOL1-G0 mice, APOL1-G1 mice manifested albuminuria increases within the first 24 hours after administration of IFN-γ (Figure 1, J and K). Therefore, we collected and characterized glomeruli from mice 24 hours after IFN-γ injection to investigate the effect of APOL1-G1 compared with APOL1-G0 in the acute phase after IFN-γ administration. At this early time point, we found that *APOL1* mRNA and protein expression were induced in both APOL1-G0 and APOL1-G1 mice, but that pathological changes were not observed by PAS staining (Figure 1L and Supplemental Figure 1B).

Downregulation of Ribosomal Genes in Glomeruli from G1xTg26 Mice of the HIVAN Model

To elucidate the molecular pathways dysregulated in glomeruli, we performed bulk RNA-seq on isolated glomeruli from HIVAN model mice (Figure 2A). Comparing Tg26 mice with WT mice, we found six upregulated and five downregulated pathways identified in the Kyoto Encyclopedia of Genes and Genomes (KEGG) (Figure 2B, Supplemental Figure 2, A and B, and Supplemental Table 4). The extracellular matrix–related pathway and focal adhesion pathways were enriched in Tg26 mice, and the ribosome pathway was downregulated in Tg26 mice (Figure 2B).

Comparing G1xTg26 with G0xTg26 mice, we found 33 upregulated and three downregulated KEGG pathways (Figure 2C and Supplemental Table 5). The Nod-like receptor signaling pathway was the top enriched pathway in G1xTg26 mice, and the ribosomal pathway was again negatively enriched in G1xTg26 mice (Supplemental Figure 2, C–E).

When comparing G0xTg26 with Tg26 mice, we found ten upregulated KEGG pathways (Supplemental Table 6). In particular, there was dysregulation of oxidative phosphorylation by APOL1-G0.

The *APOL1* mRNA expression level in glomeruli was measured by RNA-seq and was confirmed by reverse transcription-quantitative PCR (Figure 2D and Supplemental Figure 2F). The presence of the Tg26 transgene did not increase *APOL1* expression levels, despite greater albuminuria in G1xTg26 mice compared with G1 mice. Furthermore, Tg26 transgene RNA expression levels were not increased by the APOL1 high-risk variant, as confirmed by reverse transcription-quantitative PCR for the *vpr* expression level (Figure 2E and Supplemental Figure 2G).

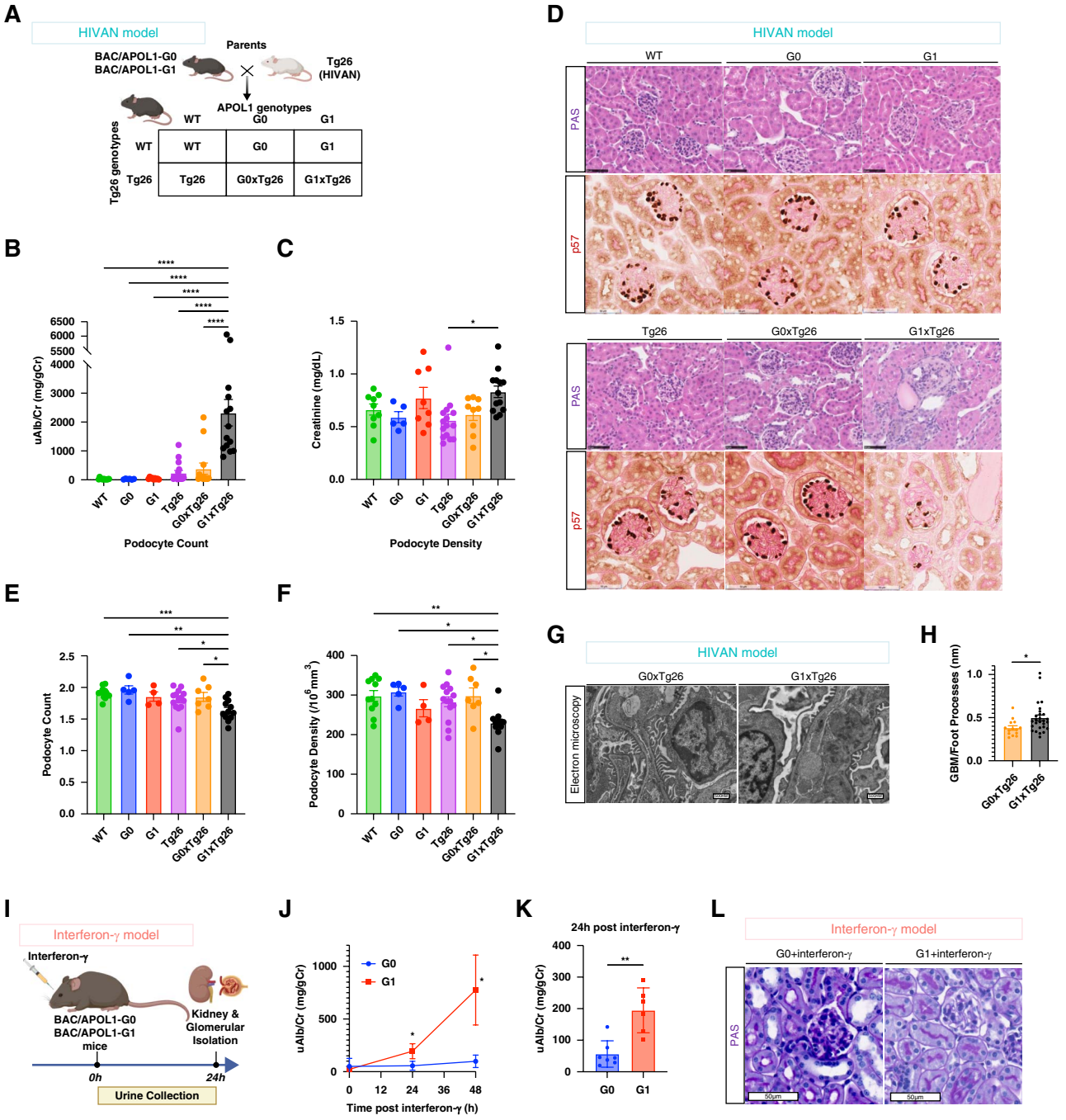

Figure 1. Characterization of the BAC/APOL1xTg26 dual transgenic HIVAN model and the IFN-γ model. (A) Overview of the HIVAN model mouse, showing six genotypes. (B and C) Plasma creatinine (mg/dl) and urinary albumin-to-creatinine ratio (mg/g creatinine) were elevated in G1xTg26 mice compared with other mice. (D) Representative hematoxylin and eosin staining images of WT, G0, G1, Tg26, G0xTg26, and G1xTg26 mouse kidneys, demonstrating glomerulosclerosis and microcystic tubular dilatation in G1xTg26 mice. p57 staining of kidney showed podocyte loss and dedifferentiation in G1xTg26 mice (scale bars are 50 μm). (E and F) Podocyte counts and densities analyzed by PodoCount shows podocyte depletion in G1xTg26 mice. (G) Electron microscopy images of glomeruli from G0xTg26 and G1xTg26 mice showed foot process effacement in G1xTg26 glomeruli (scale bars are 500 nm). (H) G1xTg26 mouse glomeruli manifested foot process effacement. Podocyte foot process width was measured (nm) in G0xTg26 and G1xTg26 mouse glomeruli, indicating a wider foot process in the latter. (I) An overview of the IFN-γ model experiment. (J) Time course of urinary albumin-to-creatinine ratios (mg/g creatinine) in the IFN-γ injection experiments, with greater albuminuria in G1 mice. (K) Urinary albumin-to-creatinine ratio increased 24 hours after IFN-γ injection in BAC/APOL1-G1 mice but not in BAC/APOL1-G0 mice. (L) PAS staining shows no apparent change in kidney histology at 24 hours after IFN-γ injection. (One-way ANOVA with Turkey's multiple comparison [B and C], one-way ANOVA with Dunnett's multiple comparison [E and F], and *t* test [H–K] were used; $^{*}P < 0.05$; $^{**}P < 0.01$; $^{***}P < 0.001$; $^{****}P < 0.0001$.) APOL1, apolipoprotein L1; BAC, bacterial artificial chromosome; GBM, glomerular basement membrane; HIVAN, HIV-associated nephropathy; PAS, periodic acid–Schiff; uAlb/CR, urinary albumin-to-creatinine ratio; WT, wild type.

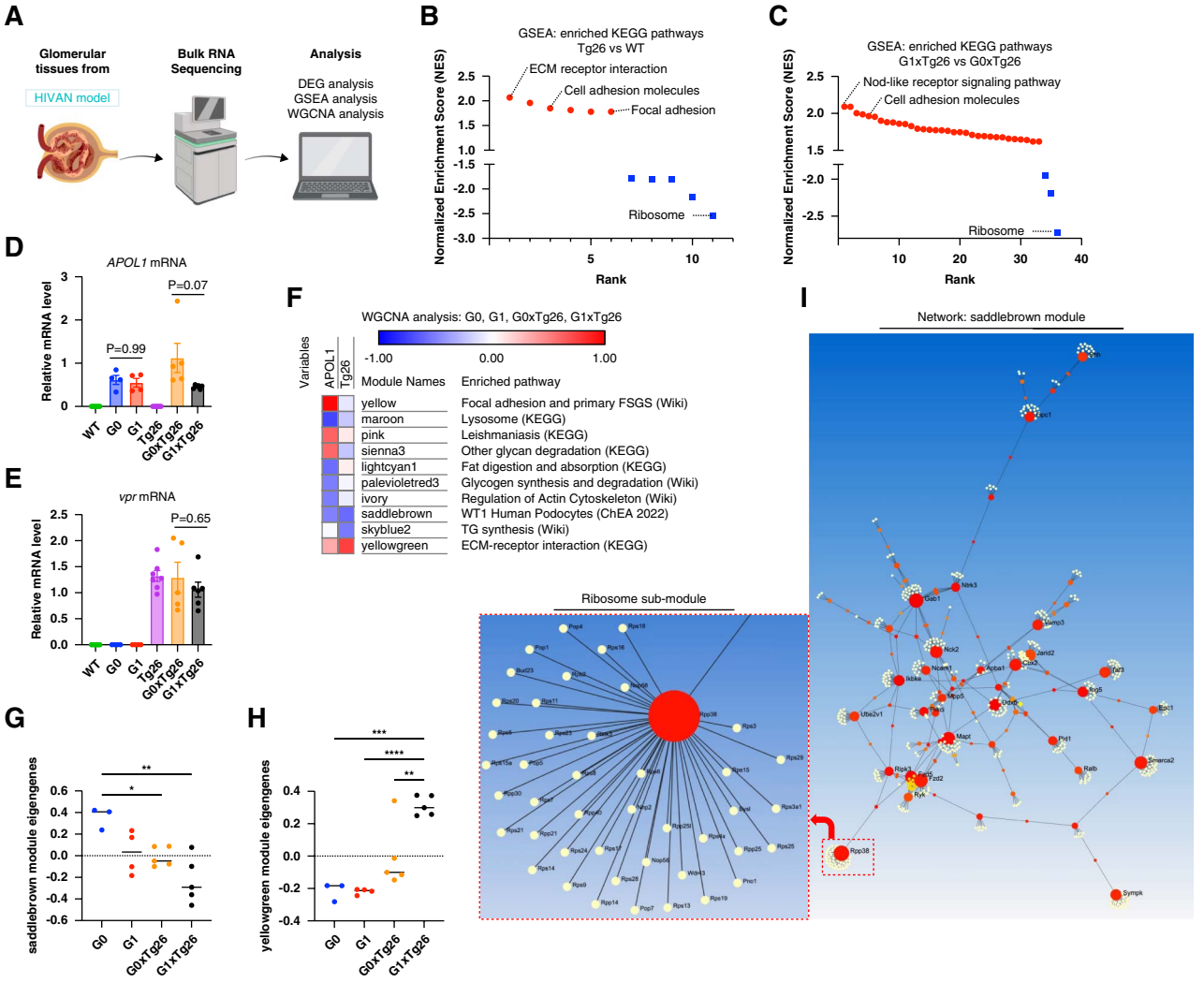

Figure 2. Bulk glomerular RNA-seq analysis results from HIVAN mouse model and control. (A) An overview of glomerular bulk RNA-seq experiments and analysis of HIVAN mouse model. (B) Waterfall plot shows GSEA results of enriched KEGG pathways, comparing Tg26 and WT mice. (C) Waterfall plot shows GSEA comparing G1xTg26 and G0xTg26 mice, with enriched KEGG pathways. (D) Relative *APOL1* mRNA levels were quantified by RT-qPCR. (E) Relative HIV-1 *vpr* mRNA levels were assessed by RT-qPCR. (F) Heatmap shows Pearson R correlation of the module eigengenes expression with *APOL*1 genotype and Tg26 genotype. Analysis involved identifying gene modules of upregulated or downregulated in HIVAN mice. Red denotes positive correlation with gene module expression, and blue denotes negative correlation with gene module expression. For example, the yellow module suggests positive correlation with APOL1-G1 mice, and genes in the yellow module were enriched in the Wiki pathway, "focal adhesion and human primary FSGS." (G) Eigengenes expression of the saddlebrown module with *APOL1* genotype and Tg26 genotype showed the lowest expression in G1xTg26 mice. (H) Eigengenes expression of the yellowgreen module with *APOL*1 genotype and Tg26 genotype showed the highest expression in G1xTg26 mice. (I) Network visualization of the saddlebrown module genes layered on to the STRING interactome generated from networkanalyst (see Methods for details). Red dots indicate highly connected hub genes that connect with many poorly connected nodes genes in yellow. The image of the ribosome submodule is magnified, showing the complexity of this network. (One-way ANOVA with Turkey's multiple comparison [D, E, G, and H] was used; $*P < 0.05$; $**P < 0.01$; $***P < 0.001$; $****P < 0.0001$.) DEGs, differentially expressed genes; ECM, extracellular matrix; GSEA, gene set enrichment analysis; KEGG, Kyoto Encyclopedia of Genes and Genomes; RNA-seq, RNA sequencing; RT-qPCR, reverse transcription-quantitative PCR; STRING, Search Tool for the Retrieval of Interacting Genes/Proteins.

Network analysis was applied to the APOL1-G0, G1, G0xTg26, and G1xTg26 datasets to identify gene modules affected by *APOL1* genotype (G1 versus G0), with or without the Tg26 transgene. Of 89 modules identified, eight modules were dysregulated by APOL1-G1 compared with APOL-G0 and three modules were dysregulated by Tg26 (Figure 2F). Notably, G0 and G1 mice lacked kidney disease and yet demonstrated different coregulated modules between G0 and G1 mice, which might have implications even in the absence of the Tg26 transgene. The saddlebrown module was the only module dysregulated significantly by both the *APOL1* genotype and the Tg26 genotype (Figure 2G). Furthermore, this module was enriched in genes reported by WT1 chromatin immuno precipitation sequencing by a previous report describing podocyte gene expression.[41]

These findings indicate that both the APOL1-G1 and the Tg26 transgene contribute to WT1 deactivation, suggesting

podocyte dedifferentiation in these two settings. Primary FSGS and lysosome pathway genes were enriched in APOL1-related modules. Extracellular matrix pathway genes were also enriched in Tg26-related modules, especially the yellowgreen module (Figure 2H).

Network visualization of saddlebrown module genes onto the Search Tool for the Retrieval of Interacting Genes/Proteins interactome showed submodule related to the ribosome KEGG pathway, which confirms downregulation of ribosomal gene expression by both APOL1-G1 and Tg26 as two hits (Figure 2I).

Single-Nuclear RNA-Seq Showed Shared IFN-γ Activation in Both Models: HIVAN and IFN-γ

To characterize molecular signatures at single-cell resolution, we conducted single-nuclear RNA-seq of isolated glomeruli from WT, G0xTg26, G1xTg26, G0+IFN-γ, and G1+IFN-γ mouse kidneys (Figure 3A). We profiled 20,276 nuclei and identified 21 cell clusters, as shown by uniform manifold approximation and projection (Supplemental Figure 3, A and B).

We selected a data subset representing 12 glomerular cell clusters. We annotated cell types on the basis of prior

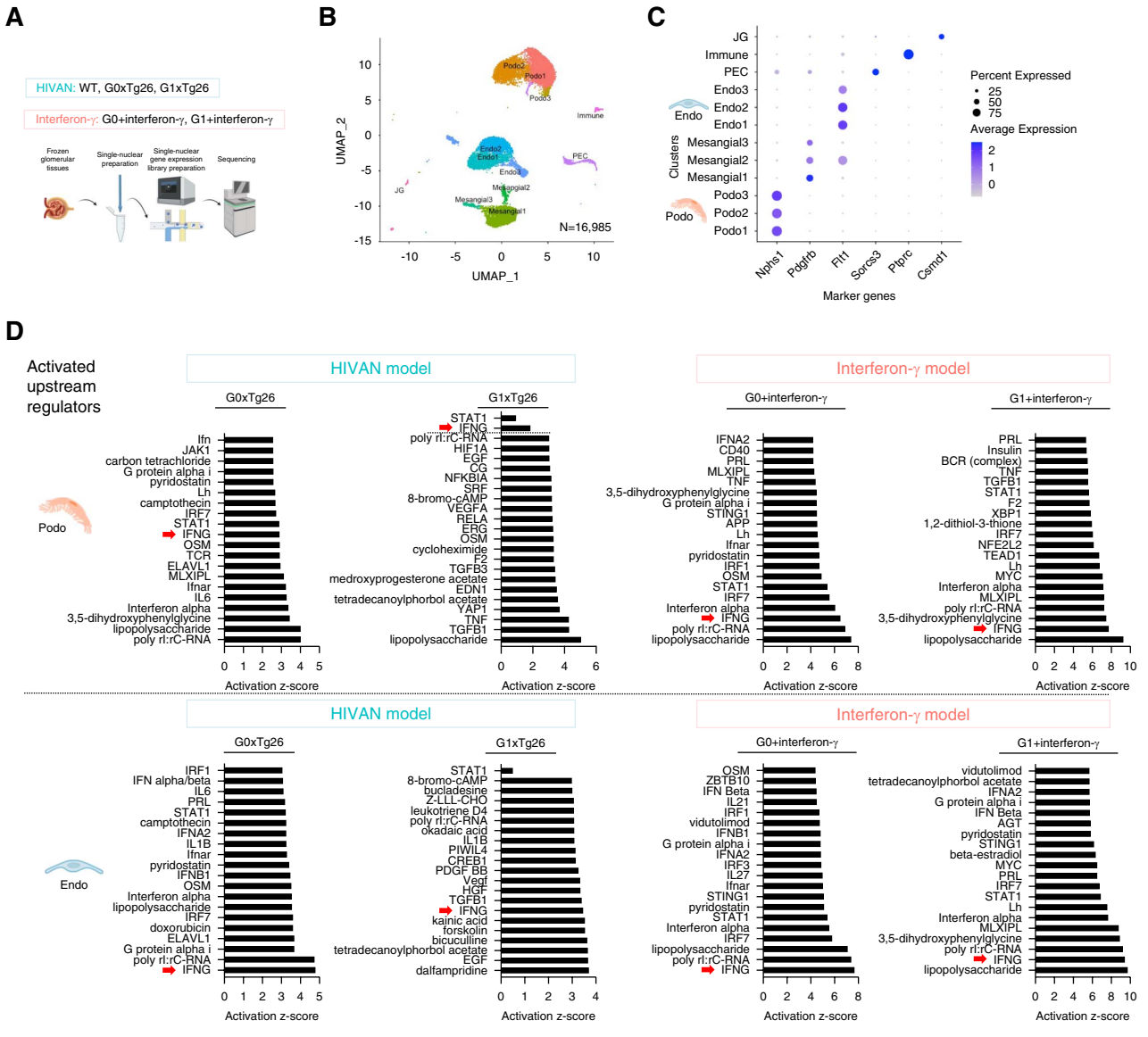

Figure 3. Glomerular single-nucleus RNA-seq experiments. (A) An overview of single-nucleus RNA-seq experiments from extracted glomeruli samples obtained from the two mouse models (HIVAN and IFN-γ), representing five distinct groups. (B) UMAP plot of single-nuclear RNA-seq data from all five samples (16,985 cells) shows 12 clusters, originating from six cell types. (C) A dot plot shows marker genes characteristic for each cluster, with the percent of cells expressing each marker genes shown by circle size and the color intensity showing the level of gene expression in each cluster; *Nphs1* for podocytes, *Pdgfrb* for mesangial cells, *Flt1* for glomerular endothelial cells, *Sorcs3* for parietal epithelial cells, *Ptprc* for immune cells, and *Csmd1* for juxtaglomerular cells. (D) Bar graphs show activation Z-scores for upstream regulators in podocytes and endothelial cells in each of the two transgenic models compared with WT mice. IFN-γ was one of the top 20 regulators in both cell types and both models, except for podocytes in G1xTg26 mice where it was a less potent regulator. UMAP, uniform manifold approximation and projection; YAP, yes-associated protein. Figure 3 can be viewed in color online at www.jasn.org.

knowledge of gene expression, including three clusters of podocytes, three clusters of mesangial cells, three clusters of endothelial cells, one cluster of parietal epithelial cells, one cluster of immune cells, and one juxtaglomerular cell cluster (Figure 3, B and C, and Supplemental Figure 3C).

APOL1 was expressed in podocytes and glomerular endothelial cells (Supplemental Figure 3D). HIV genes were relatively highly expressed in podocytes compared with other glomerular cell types (Supplemental Figure 3E). Immune cells were more frequent in G1xTg26 mice compared with G0xTg26 mice, which was confirmed by F4/80-positive macrophage staining (Supplemental Figure 3, B and F). Regarding all nine glomerular cell clusters, we regrouped these into three new groups, comprising podocytes, endothelial cells, and mesangial cells.

Using these clusters, we conducted differential expression analysis and upstream regulator analysis comparing all models with WT (Figure 3D). Both podocytes and endothelial cells in the IFN-γ model showed that IFN-γ was one of the top upstream regulators, which confirms the model's validity. Both podocytes and endothelial cells in the G0xTg26 HIVAN model showed that IFN-γ was one of the top upstream regulators together with poly I:C-RNA, indicating a direct effect of HIV transgenes. In comparison, podocytes in the G1xTg26 model had moderate activation of IFN-γ and higher activation of fibrogenesis factors, such as TNF, TGFβ1, and yes-associated protein (Figure 3D).

Podocyte Damage Patterns by APOL1-G1: Mammalian Target of Rapamycin and Eukaryotic Translation Initiation Factor 2

To define cellular-specific DEGs by APOL1 genotype within the two models, we conducted differential expression analysis comparing G1xTg26 with G0xTg26 (HIVAN) mice and G1+IFN-γ with G0+IFN-γ (IFN-γ) mice. Thus, we created four DEG sets: Podo_APOL1_HIVAN (n=417); Podo_APOL1_IFN-γ (n=949); Endo_APOL1_HIVAN (n=166); and Endo_APOL1_IFN-γ (n=804).

IPA pathway analysis on the basis of these podocyte DEG sets identified pathways dysregulated in the podocyte cell cluster in two different models, HIVAN and IFN-γ (Figure 4, A and B). Comparison of pathway activity by APOL1 variant in each model is shown (Figure 4C). The mammalian target of rapamycin (mTOR) pathway was activated in APOL1-G1 mice of both models. Specifically, the mammalian target of rapamycin complex 1 signaling pathway was activated in APOL1-G1 podocytes, as shown by increased downstream phospho-rpS6 and phospho-4E-BP (Figure 4D). Because the mTOR pathway contributes to glomerulosclerosis,[42] mTOR activation in podocytes by APOL1-G1 may contribute to glomerular injury.

The eukaryotic translation initiation factor 2 (EIF-2) pathway was the top canonical pathway dysregulated in podocytes in both models, with different directionality. In this pathway, the IFN-γ model manifested *activation* (active Z-score 4.85) while the HIVAN model manifested *deactivation* (active Z-score -2.53). These findings suggest that the effect of the APOL1 variant on the EIF-2 pathway may be context dependent. Notably, genes encoding ribosomal proteins are components of the EIF-2 pathway. Ribosomal protein S6, one of the genes differentially regulated in the EIF-2 pathway, showed decreased expression in G1xTg26 mice and increased expression in G1+IFN-γ mice (Figure 4D).

When we compared DEG sets obtained from podocytes in the two models (Figure 4E), we identified 178 shared DEGs in both models. Of 178 DEGs shared, 84 DEGs were upregulated in both models (Podo_APOL1_Pos, [n=84]). There were 330 upregulated DEGs in the HIVAN model (Podo_APOL1_ HIVAN_Pos [n=330]) and 684 in the IFN-γ model (Podo_APOL1_ IFN-γ_Pos DEG gene set [n=684]). These upregulated podocyte DEGs had positive enrichment in bulk RNA-seq data, comparing G1xTg26 with G0xTg26 mice and G1 with G0 mice (Supplemental Figure 4, A–C). On the other hand, endothelial DEGs did not show strong enrichment in bulk RNA-seq data compared with podocyte DEGs (Supplemental Figures 5, A–C, and 6A). This suggests that glomerular bulk RNA-seq captures podocyte signatures relatively well, but not endothelial cell signatures.

Comparing Podocyte Damage Patterns by APOL1-G1 in Mouse Models with Human, *Ex Vivo*, and *In Vitro* Data

To extrapolate the relevance of these data to human disease, we conducted GSEA using publicly available human glomerular RNA-seq datasets with *APOL1* genotype information.[37] We then asked whether the mouse DEGs were also enriched in the human RNA-seq dataset.

The DEG set from HIVAN mouse model podocytes (Podo_APOL1_ HIVAN_Pos [n=330]) had positive enrichment in RNA-seq data (Figure 4F). By contrast, the DEG set from the mouse IFN-γ model podocytes (Podo_APOL1_ IFN-γ_Pos [n=684]) had negative enrichment in RNA-seq data (Figure 4F). *Positive gene enrichment* refers to genes whose glomerular expression was higher in human APOL1 high-risk kidneys compared with human APOL1 low-risk kidneys. *Negative gene enrichment* refers to genes whose expression was lower in human APOL1 high-risk kidneys compared with human APOL1 low-risk kidneys. These findings indicated that HIVAN model podocytes had similar transcriptomic signatures by APOL1 variant to the human FSGS glomeruli, as reflected in human glomerular transcriptomes.

We also compared these transgenic mouse model data with urinary single-cell RNA-seq data from patients with FSGS (*ex vivo*)[39] and with bulk RNA-seq of podocyte cell lines (*in vitro*).[40] We conducted IPA pathway analysis on the basis of DEGs, comparing APOL1 G1/G2 podocyte RNA with APOL1 G0/G0 podocyte RNA, using both human urine single-cell data and human podocyte cell data. Both comparisons showed the EIF-2 pathway as the most dysregulated pathway, with an activated pathway z-score of 2.4 (urinary single-cell data) (Figure 4G) and 5.4 (podocyte cell-line data) (Figure 4H). Both pathway scores were similar to those of the IFN-γ mouse model.

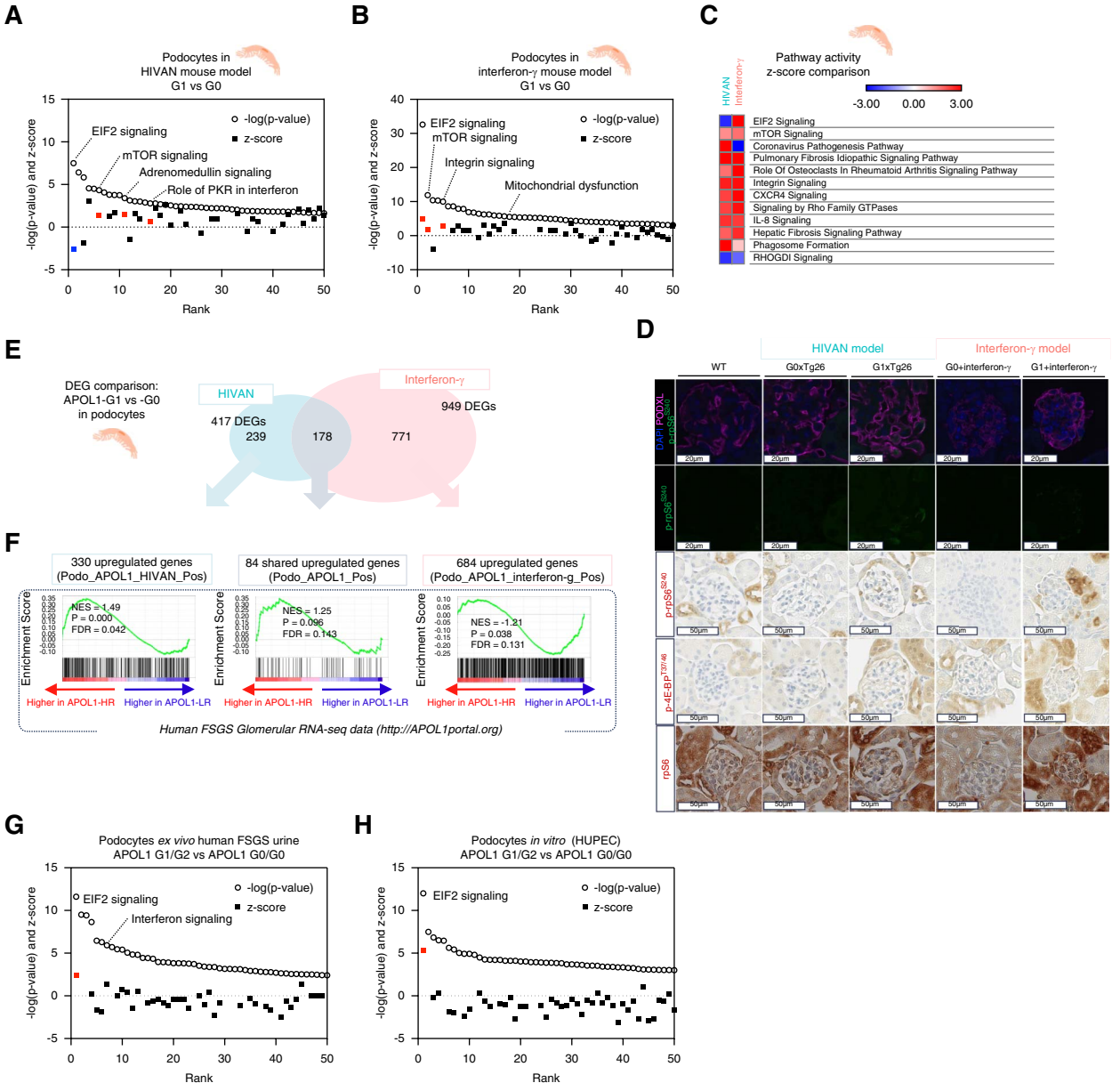

Figure 4. Single-nucleus RNA-seq data analysis in podocytes. (A) A waterfall plot of IPA pathways enriched by DEGs from podocytes comparing APOL1-G1 and APOL1-G0 in the HIVAN model shows mTOR activation and EIF-2 signaling deactivation in G1 podocytes. (B) A waterfall plot of IPA pathways enriched by DEGs from podocytes comparing APOL1-G1 and APOL1-G0 in the IFN-γ model shows mTOR and EIF-2 signaling activation in APOL1-G1 podocytes. (C) A heatmap shows active Z-score comparing *APOL1* genotype (G1 versus G0) in the HIVAN and IFN-γ models. (D) Representative images of both immunofluorescence staining and immunoperoxidase staining of two phosphoproteins (phospho-rpS6 and phospho-4E-BP1) and a protein (RPS6), demonstrating expression in podocytes. These indicate mTOR activation in APOL1-G1 podocytes but not in APOL1-G0 podocytes. (E) Venn diagram of DEGs, comparing *APOL1* genotype (G1 versus G0) in both HIVAN and IFN-γ model podocytes. (F) Enrichment plot of Podo_APOL1_HIVAN_Pos genes (*i.e.*, upregulated podocyte genes in the HIVAN model comparing APOL1- G1 versus APOL1-G0) (left panel) and Podo_APOL1_Pos genes (*i.e.*, upregulated podocyte genes in the both models comparing APOL1-G1 versus APOL1-G0) (middle panel) show positive enrichment in human glomerular RNA-seq comparing APOL1-HR and LR (http://APOL1portal.org). Podo_APOL1_IFN-γ_Pos (*i.e.*, upregulated podocyte genes in the IFN-γ model comparing APOL1-G1 versus APOL1-G0) (right panel) shows negative enrichment. (G) Waterfall plot of IPA pathways enriched by DEGs from podocytes *ex vivo* human FSGS urine single-cell RNA-seq data comparing APOL1-G1/G2 samples and G0/G0 samples (GEO accession number GSE176465), shows EIF-2 signaling activation in G1/G2 podocytes. (H) A waterfall plot of IPA pathways enriched by expression of DEGs obtained from podocytes *in vitro* comparing APOL1-G1/G2 and G0/G0 cells (GSE194337). This shows EIF-2 signaling activation in G1/G2 podocytes. DAPI, 4′,6-diamidino-2-phenylindole; EIF-2, eukaryotic translation initiation factor; GEO, gene expression omnibus; HR, high-risk genotype; IPA, ingenuity pathway analysis; LR, low-risk genotype; mTOR, mammalian target of rapamycin; PKR, protein kinase R; RPS6, ribosomal protein S6.

Although the IFN-γ mouse model signature in podocytes differed from that of human FSGS glomeruli, the IFN-γ mouse model may be mimicking the effect of APOL1 risk variants in the context of IFN-γ surge in humans, which was observed in urinary single-cell RNA-seq (*ex vivo*) data and podocyte cell-line (*in vitro*) data.

Common Podocyte Damage Patterns by APOL1-G1 in HIVAN and IFN-γ Models

A shared DEG set in these two models (Podo_APOL1_Pos [n=84]) had a positive trend toward enrichment in human RNA-seq data, although it did not reach significance (Figure 4F). These genes merit further investigation

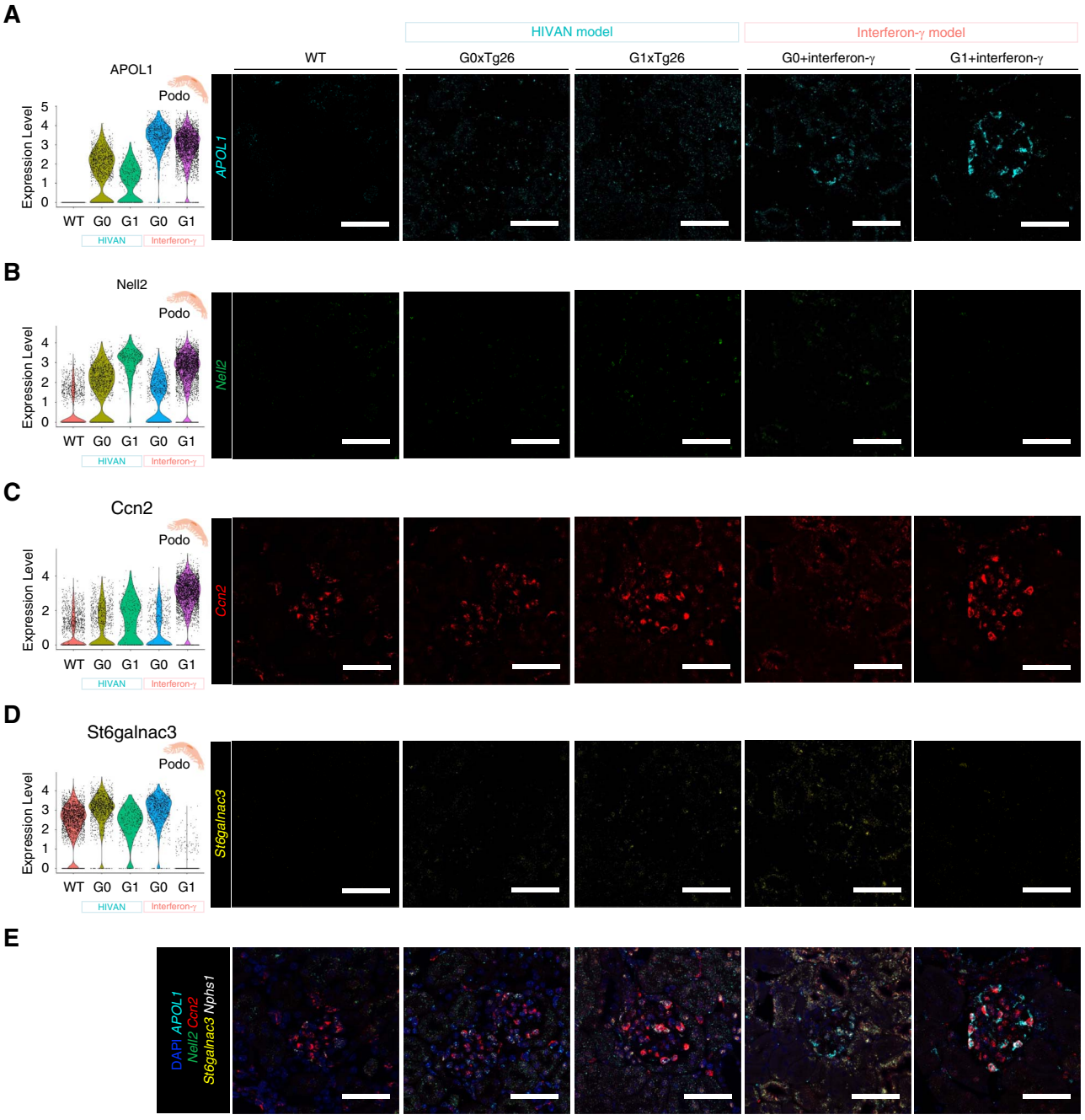

Figure 5. RNA expression of *APOL1* and potential markers of podocyte injury, *Nell2*, *Ccn2*, and *St6galnac3*. (A) Violin plot shows *APOL1* expression in podocytes obtained from snRNA-seq data and paired with corresponding FISH images of *APOL1* mRNA probed in cyan. After IFN-γ exposure, *APOL1* expression increased in APOL-G0 and APOL1-G1 transgenic mice. (B) Violin plot shows *Nell2* expression in podocytes obtained from snRNA-seq data and corresponding FISH images of *Nell2* mRNA probed in green. (C) Violin plot shows *Ccn2* (CTGF) expression in podocytes obtained from snRNA-seq data and corresponding FISH images of *Ccn2* mRNA probed in red. (D) Violin plot shows *St6galnac3* expression in podocytes obtained from snRNA-seq data and corresponding FISH images of *St6galnac3* mRNA probed in yellow. (E) FISH overlay images showing targets including DAPI in blue color and *Nphs1* mRNA probed in white (scale bars are 50 μm). CTGF, connective tissue growth factor; FISH, fluorescent *in situ* hybridization; snRNA-seq, single-nucleus RNA-sequencing.

because they are potential contributors to APOL1 variant–induced damage patterns in a podocyte-specific manner, and there was robust expression of *APOL1* in podocytes *in vivo* (Figure 5A).

One DEG was *Nell2*, encoding neural EGF-like 1, which is an axon guidance cue; its antiligand is *Robo3*, expressed in endothelial cells.[43] *Nell2* was upregulated in podocytes in both models, as shown by single-nucleus RNA-sequencing

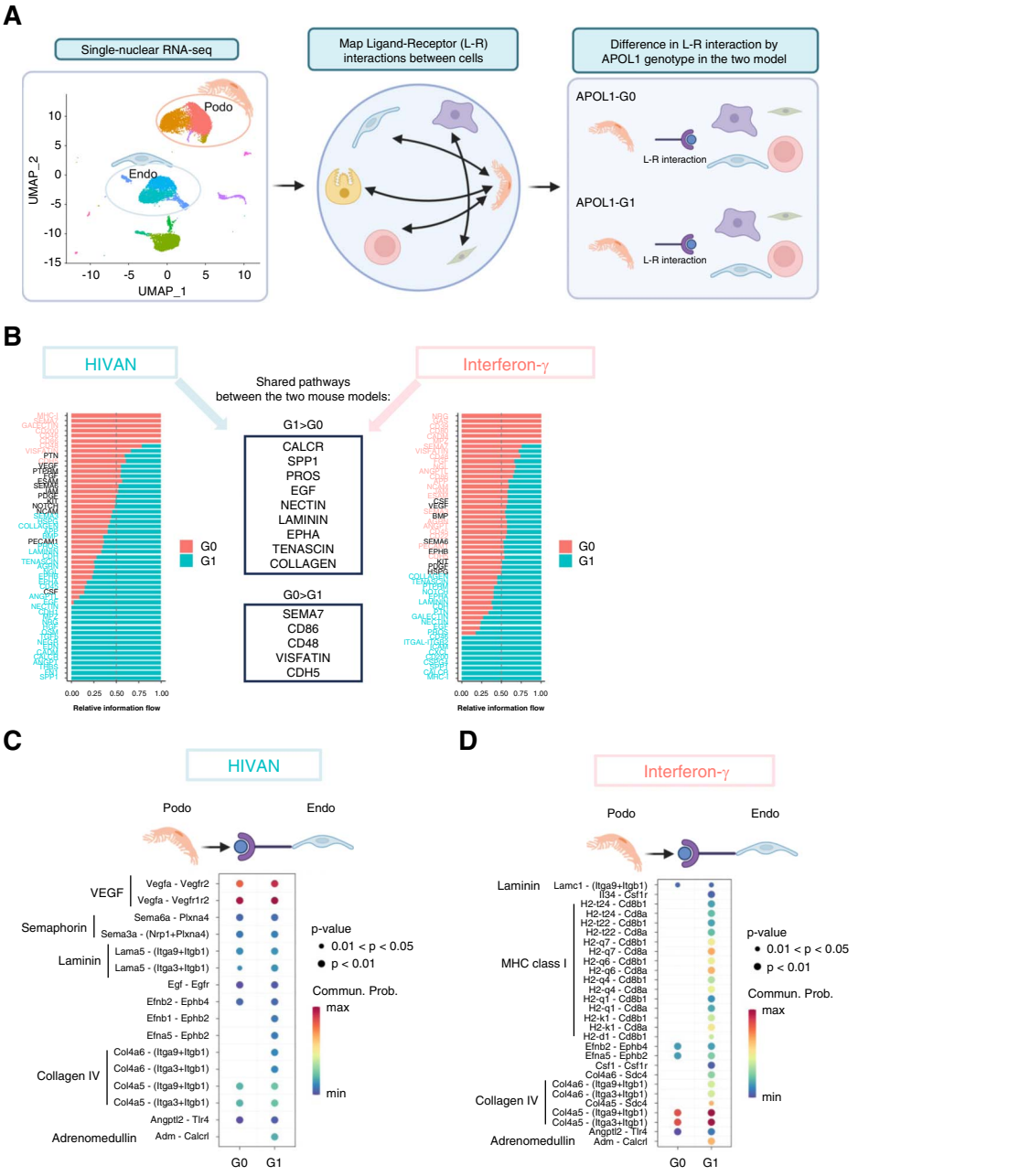

Figure 6. Cell–cell interaction analysis showing differential interactions between APOL1-G1 and -G0 in two models. (A) Schematic images show the flow of cell–cell interaction analyses. (B) A waterfall plot of pathways shows relative information flow between APOL1-G1 and APOL1-G0 mice in the HIVAN and IFN-γ models. The boxes show common pathways dysregulated in both transgenic models. (C) The dot plot shows predicted upregulated signaling from podocytes to endothelial cells in APOL1-G1 mice compared with APOL1-G0 mice in the HIVAN model. (D) The dot plot shows predicted upregulated signaling from podocytes to endothelial cells in APOL1-G1 mice compared with APOL1-G0 mice in the IFN-γ model. (E) Violin plot shows expression of *Adm*, encoding adrenomedullin, in podocytes obtained from snRNA-seq data. (F) The dot plot shows predicted upregulated signaling from endothelial cells to podocytes in APOL1-G1 mice compared with APOL1-G0 mice in the HIVAN model. (G) The dot plot shows predicted upregulated signaling from endothelial cells to podocytes in APOL1-G1 mice compared with APOL1-G0 mice in the IFN-γ model. (H) Violin plot shows *Dag1* expression in podocytes obtained from snRNA-seq data. (I) Violin plot shows *H2-K1*, *H2-D1* expression in podocytes obtained from snRNA-seq data. (J) Violin plot shows *Efnb2* expression in endothelial cells obtained from snRNA-seq data. Figure 6 can be viewed in color online at www.jasn.org.

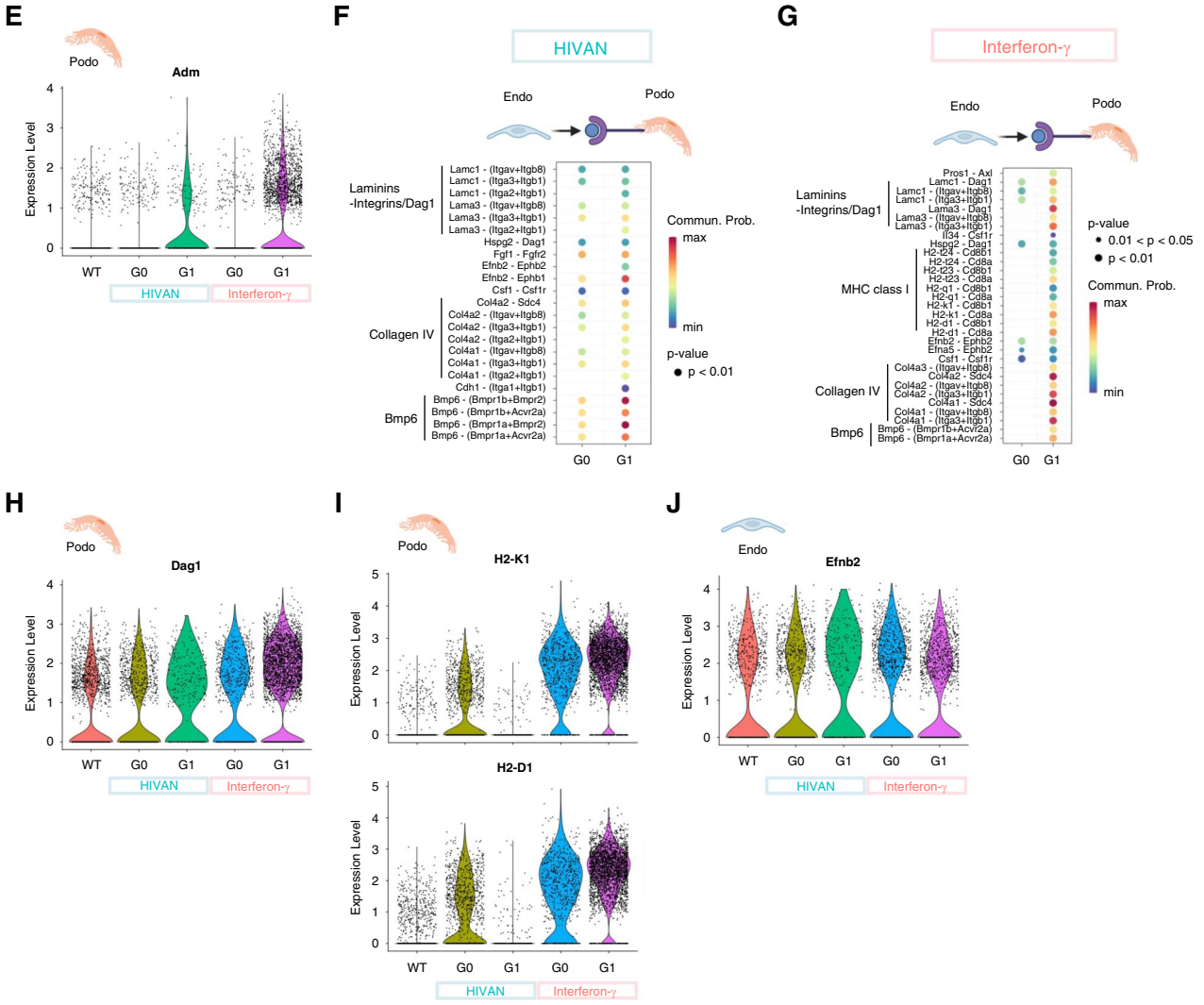

Figure 6. *Continued.*

and ISH (Figure 5B), indicating detachment of podocyte foot processes from GBM, as it has been shown in the similar context in neuronal synapses.[44] Another DEG was *Ccn2* (Figure 5C), a known profibrotic factor in the kidney.[45,46] *Ccn2* can be a marker of glomerulosclerosis. One of the DEGs downregulated in G1 was *St6galnac3* (Figure 5D), which is a member of the family of sialyltransferases that transfer sialic acids from cytidine monophosphate–sialic acid to glycoproteins and glycolipids.[47] Low *St6galnac3* expression is a marker of impaired sialylation, as shown in a human disease and mouse model of FSGS.[48,49]

Cell–Cell Interaction Analysis Characterized Podocyte–Endothelial Communications in APOL1-G1 Mice

APOL1 high-risk variant expressed in podocytes drives podocytopathy. However, roles for other cells in glomerulopathy remain to be identified. Using single-nuclear RNA-seq data, we conducted cell–cell interaction analysis and characterized potential dysregulated interactions among cell types (Figure 6A). When information flow was quantified and compared within each model, we found nine common pathways upregulated in G1 and five common pathways downregulated in G1 (Figure 6B). When we identified increased signals from podocytes to endothelial cells (Figure 6, C and D), adrenomedullin (*Adm*) to calcitonin receptor-like receptor (*Calcrl*) signaling was robustly upregulated in both models, mainly driven by upregulation of *Adm expression* in mouse podocytes (Figure 6E). Adrenomedullin is a potent vasoactive substance that is produced abundantly in vascular endothelial and smooth muscle cells.[50,51] Adrenomedullin is upregulated following podocyte injury induced by puromycin aminonucleoside[52] and is protective against ROS-induced podocyte injury.[53] Adrenomedullin upregulation may also protect endothelial cells through interaction with calcitonin receptor–like receptor during APOL1-induced kidney injury.

We identified increased signals from endothelial cells to podocytes (Figure 6, F and G). The laminin subunit α 3 *(Lama3)–dystroglycan (Dag1)* interaction was upregulated, mainly by upregulation of *Dag1* in podocytes (Figure 6H). Dystroglycan is highly abundant at the interface between the podocyte foot process and the GBM.[54] Podocyte

dystroglycan may support podocyte adhesion to GBM laminin,[55] so upregulation of *Dag1* may indicate early focal adhesion formation in APOL1-induced kidney injury. It is also noteworthy that the MHC class 1 pathway was upregulated by IFN-γ but downregulated in the HIVAN model. As MHC class 1 expression in podocytes is induced by IFN-γ[56] and inhibited by HIV accessory proteins *Nef* and *Vpu*,[57] these findings indicated differential immune responses in podocytes by APOL1 variant in each disease condition (Figure 6I). Furthermore, we found that ephrin-B2 (*Efnb2*), an endothelial cell–expressed gene was expressed more highly in G1xTg26 mice compared with all other genotype mice. This protein is a ligand for the ephrin type-B receptor 1 (*Ephb1*), which is expressed in podocytes (Figure 6, I and J).

Of interest, there were 178 upregulated or downregulated genes that were shared between the HIVAN model and the IFN-γ model in podocytes (Figure 7A). By contrast, there were 65 upregulated or downregulated genes in endothelial cells that were shared in the two models. Furthermore, 20% of IFN-model differentially expressed genes were also expressed as HIVAN model podocytes, whereas only 8% of IFN-γ model differentially expressed genes were shared with the HIVAN model in endothelial cells. These differences confirm the central role of IFN-γ in APOL1-mediated podocyte injury.

Zbtb16 May Be an Intermediate Regulator in APOL1 Variant–Induced Glomerular Injury

Transcription factors, such as WT1, can drive podocyte differentiation. Furthermore, loss of certain transcription factors can be detrimental to podocyte function. We examined downregulated DEGs in the HIVAN and IFN-γ models

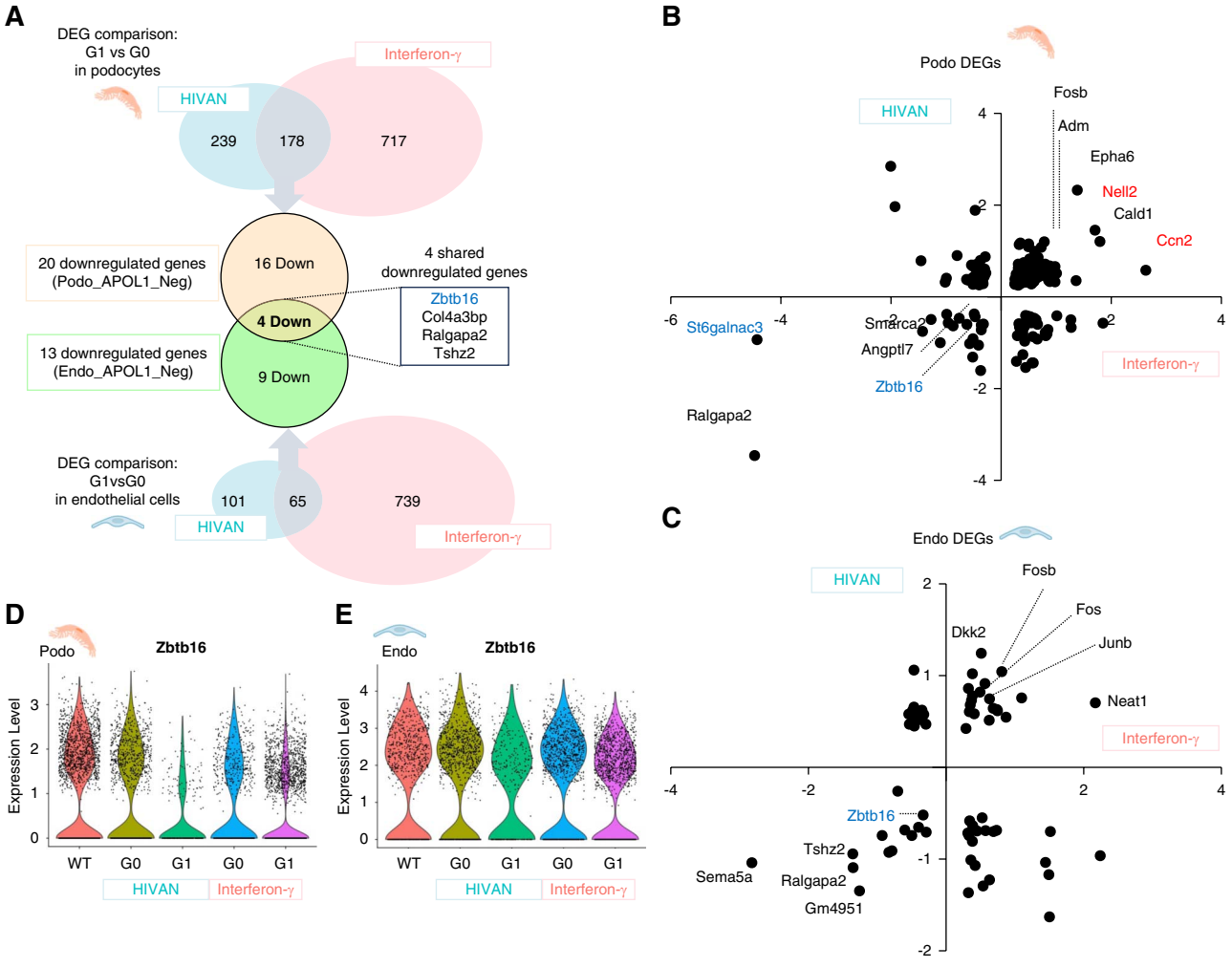

Figure 7. Zbtb16 was a common downregulated gene in APOL1-G1 compared with APOL1-G0 in two models and two cell types. (A) Venn diagram of DEGs, comparing APOL1 genotype (G1 versus G0) in both the IFN-γ model and the HIVAN model and in both podocytes and glomerular endothelial cells. There were four downregulated genes shared by the two models, as shown in the box. (B) Scatter plot of DEGs in podocytes compared with APOL1-G1 and APOL1-G0 mice was plotted by log2 fold change in the IFN-γ model (*x* axis) and the HIVAN model (*y* axis). (C) Scatter plot of DEGs in endothelial cells compared with APOL1-G1 and APOL1-G0 mice was plotted by log2 fold change in the IFN-γ model (*x* axis) and the HIVAN model (*y* axis). (D) Violin plot shows *Zbtb16* expression in podocytes obtained from snRNA-seq data. (E) Violin plot shows *Zbtb16* expression in endothelial cells obtained from snRNA-seq data. Figure 7 can be viewed in color online at www.jasn.org.

in both podocytes and endothelial cells (Figure 7A), and we identified four downregulated DEGs—*Zbtb16*, *Col4a3bp*, *Ralgapa2*, and *Tshz2*. *Zbtb16* was recently reported to be the most important transcription factor in dexamethasone-induced podocyte protection.[58] *Zbtb16* is induced by dexamethasone and is downregulated in collapsing FSGS. The two mouse models showed downregulation of *Zbtb16* in both cell types, podocytes and endothelial cells (Figure 7, B–E). This may indicate cytoskeletal disturbance and glucocorticoid resistance in APOL1-induced nephropathy in transgenic mice, possibly in both cell types.

Discussion

We characterized two models: HIVAN and IFN-γ administration using BAC/APOL1 mice expressing APOL1. Both models showed accelerated glomerular disease in APOL1-G1 compared with APOL1-G0 mice. Single-nucleus RNA-seq of these models highlighted differences and common pathways dysregulated by APOL1-G1 compared with APOL1-G0 in these models, at cellular resolution. This unbiased approach identified DEGs that are potential disease markers or mediators of APOL1 nephropathy.

The HIVAN mouse model with human APOL1 expression from a BAC transgene provided an approach to investigate APOL1 variant–specific molecular pathways. Owing to F1 strain background of this HIVAN model (Supplemental Figure 8), we observed a milder phenotype induced by the Tg26 transgene compared with Tg26 mice on an Friend virus B NIH background, which is congruent with a previous report.[59] Thus, the current HIVAN model is suitable model to study transcriptional change happening earlier in the disease course by APOL1-G1. The present mice exhibited greater albuminuria and fewer podocytes induced by the combination of the HIV Tg26 transgene and *APOL1*-G1 gene, compared with Tg26 alone. A trend in lower podocyte density in APOL1-G1 mice might indicate synergistic mechanisms in G1xTg26 mice. APOL1-G1xTg26 mice manifested greater albuminuria and fewer podocytes compared with APOL1-G0xTg26 mice.

In the present HIVAN model, we did not observe robust induction of APOL1 transgene expression by the HIV transgene. We speculate that chronic activation of the IFN-γ pathway in Tg26 mice may downregulate APOL1 expression in podocytes and endothelial cells. Another possibility is that we could not capture episodic APOL1 upregulation due to the cross-sectional study design. HIV transgene expression was also not induced by APOL1 expression. HIV transgenes showed rather the trend of downregulation by APOL1-G1 expression, which is similar to the report of HIV transgene downregulation by APOL1-G0 expression.[60]

APOL1-G1 variant induced transcriptomic differences, revealed by bulk and single-nucleus RNA-seq. HIV gene expression drove additional perturbations, such as activation of extracellular matrix–related pathways. Ribosome pathway genes were downregulated by both APOL1-G1 genotype and the Tg26 HIV transgene. Nod-like signaling pathway activation by APOL1-G1 shown here was congruent with previous reports reporting on nod-like receptor protein activation by APOL1 risk variants.[10,61]

By contrast, administration of IFN-γ to BAC/APOL1 mice represents an acute APOL1 induction model and increased *APOL1* mRNA and protein expression in podocytes and glomerular endothelial cells, with greater expression in podocytes. The IFN-γ model was robust, as previously reported.[7,16] APOL1 mRNA and protein were upregulated in both APOL1-G0 and APOL1-G1 mice, but albuminuria was induced only in APOL1-G1 mice. APOL1 is toxic *in vitro* and *in vivo*, when expressed at supraphysiologic levels.[9,62] In the NEPTUNE study of glomerular disease, *APOL1* high-risk patients had higher *APOL1* gene expression in glomeruli compared with APOL1 low-risk patients.[37] Albuminuria was induced in APOL1-G1 mice but not in APOL1-G0 mice. Thus, increased expression of APOL1-G1 in podocytes likely induces albuminuria.

By comparing two different models, we made novel observations concerning APOL1 nephropathy. Comparing podocyte DEGs in both models (HIVAN and IFN-γ), the mTOR pathway was activated in APOL1-G1 mice of both HIVAN and IFN-γ models. As with other shared pathways activated in both models, this could be a therapeutic target. The mTOR pathway contributes to glomerular hypertrophy[63] and glomerulosclerosis.[42]

Comparison with NEPTUNE glomerular RNA-seq data, GSEA indicated that the HIVAN model manifested a transcriptome that was close to the human (non-HIV) FSGS transcriptome, when comparing *APOL1* high-risk and low-risk genotypes.

We found negative gene enrichment of the Podo_APOL1_IFN-γ_Pos gene set in human FSGS RNA-seq data comparing *APOL1* genotypes. One possible explanation is that the mice were studied 24 hours after IFN-γ administration, whereas human studies involve chronic exposure to the IFN-γ pathway activation. The IFN-γ model is an APOL1 induction model. Similar IFN-γ–related human diseases have not been characterized at a molecular level in this early stage. Interestingly, the EIF-2 pathway manifested mirror images in the two models. The EIF-2 pathway was downregulated in HIVAN by APOL1-G1 variant, whereas the EIF-2 pathway was activated in the IFN-γ model by APOL1-G1 variant. Furthermore, EIF-2 pathway activation by APOL1 high-risk variant resembles urine single-cell RNA-seq and human podocyte cell lines. Clinically, *APOL1* gene induction may be either episodic or sustained, leading to kidney disease. This might explain the transcriptomic differences between the HIVAN model and the interferon-γ model. EIF-2 and mTOR pathways are essential in protein translation and ribosomal gene transcription. Dysregulation of either pathway can be the result of feedback from other perturbations in closely related pathways, such as the protein kinase R pathway.[14] This was confirmed here.

We found genes manifesting either increased or decreased expression in both HIVAN and IFN-γ models and which were dysregulated in APOL1-G1 mice compared with APOL1-G0 mice. If replicated in human kidney samples, these genes might be markers of APOL1-specific podocytopathy. For example, *Ccn2*, encoding cellular network communication factor 2, is a profibrogenic factor and a possible marker of podocyte fibrogenic status. *St6galnac3* is a family of sialyltransferases that transfer sialic acids to

glycoproteins and glycolipids. Measuring the podocyte RNA expression of *St6galnac3* or finding defective sialylation could be an early marker to identify APOL1 variant–induced podocytopathy.[48] How the APOL1-G1 variant downregulates *St6galnac3* requires further investigation. Similarly, through cell–cell interaction analysis, adrenomedullin and dystroglycan were identified as candidate markers of APOL1 podocytopathy. Furthermore, we found endothelial *Efnb2* expression was upregulated in G1xTg26 mice compared with other genotype mice. Ephrin receptor-ligand signaling is involved in kidney fibrosis[64] and angiogenesis.[65] These genes also warrant further investigation.

Zbtb16 mRNA expression was downregulated in podocytes and endothelial cells in both the HIVAN and IFN-γ models. Glucocorticoid-resistant nephrotic syndrome has both genetic causes and nongenetic causes; the former includes APOL1 high-risk variants.[66,67] The present finding may elucidate mechanisms of glucocorticoid resistance in APOL1-driven kidney diseases.

We identified three podocyte clusters by unbiased clustering. Upon characterizing marker genes (Supplemental Figure 7C), we found that the Podo2 cluster had high expression of ribosomal protein genes. The Podo3 cluster had high expression of HIV genes (Supplemental Figure 3E) and APOL1-G1 variant–induced genes, such as *Nell2*, as described. We speculate that the Podo3 subcluster represents the podocyte subcluster most dysregulated by APOL1 risk variants.

We acknowledge limitations of this study. BAC/APOL1 mice manifest different kidney APOL1 expression levels among genotypes.

In conclusion, we have characterized APOL1 transgenic mouse models to investigate cell-specific genes and pathways involved in APOL1 G0 and G1 variant–induced glomerular diseases. The HIVAN and IFN-γ models showed distinct APOL1-G1–specific transcriptomic patterns compared with APOL1-G0 mice. This identified genes differentially expressed between APOL1-G0 and APOL1-G1 mice. These genes are potential APOL1 variant–specific therapeutic targets.

Disclosures

Disclosure forms, as provided by each author, are available with the online version of the article at http://links.lww.com/JSN/E685.

Funding

J.B. Kopp: National Institute of Diabetes and Digestive and Kidney Diseases (1ZIADK043411). C.A. Winkler: National Cancer Institute (75N91019D00024).

Acknowledgments

We thank the Sequencing Facility and Bioinformatics Group (Frederick National Laboratory for Cancer Research (FNLCR), NCI, NIH) for sequencing and informatics support, Kris Ylaya (NCI/NIH) and Maria Campos (NEI/NIH) for pathological service, Patricia Zerfas (OD/NIH) for electron microscopic service, Dr. Koji Okamoto (Tohoku University, JAPAN) for scientific suggestions, and Drs. Jurgen Heymann and Luis Menezes (NIDDK/NIH) for critical manuscript review. We appreciate receiving BAC/APOL1 mice from Merck Sharp and Dohme LLC, Rahway, NJ. We appreciate receiving APOL1 antibodies from Genentech, South San Francisco, CA. This work utilized the resources of the NIH HPC Biowulf cluster (http://hpc.nih.gov) and NIDDK Advanced Light Microscopy and Image Analysis Core (ALMIAC) and NIDDK Mouse Transgenic Core Facility and NEI Histology Unit/Biological Imaging Core Facility. Figures were created with Morpheus (https://software.broadinstitute.org/morpheus) and BioRender.com. Part of this work was presented at 14th International Podocyte Conference and 32nd NKF Annual Fellows Research Forum. The content of this publication does not necessarily reflect the views or policies of the Department of Health and Human Services, nor does mention of trade names, commercial products, or organizations imply endorsement by the US Government.

Author Contributions

Conceptualization: Teruhiko Yoshida.
Data curation: Teruhiko Yoshida.
Formal analysis: Paride Fenaroli, Khun Zaw Latt, Avi Z. Rosenberg, Briana A. Santo, Teruhiko Yoshida, Yongmei Zhao.
Funding acquisition: Jeffrey B. Kopp, Cheryl A. Winkler.
Investigation: Joon-Yong Chung, Shashi Shrivastav, Teruhiko Yoshida.
Methodology: Joon-Yong Chung, Avi Z. Rosenberg, Teruhiko Yoshida.
Resources: Joon-Yong Chung, Stephen M. Hewitt, Jeffrey B. Kopp, Pinaki Sarder, Vincent M. Tutino, Cheryl A. Winkler.
Software: Avi Z. Rosenberg, Briana A. Santo, Pinaki Sarder.
Supervision: Stephen M. Hewitt, Jeffrey B. Kopp, Pinaki Sarder, Vincent M. Tutino, Cheryl A. Winkler, Yongmei Zhao.
Visualization: Teruhiko Yoshida.
Writing – original draft: Teruhiko Yoshida.
Writing – review & editing: Joon-Yong Chung, Paride Fenaroli, Stephen M. Hewitt, Jeffrey B. Kopp, Khun Zaw Latt, Avi Z. Rosenberg, Pinaki Sarder, Shashi Shrivastav, Vincent M. Tutino, Cheryl A. Winkler, Teruhiko Yoshida, Yongmei Zhao.

Data Sharing Statement

https://www.ncbi.nlm.nih.gov/geo/query/acc.cgi?acc=GSE227234, https://www.ncbi.nlm.nih.gov/geo/query/acc.cgi?acc=GSE227235. Original data files and count tables have been deposited in GEO (GSE227234, GSE227235). Other data are available from the authors upon request.

Supplemental Material

This article contains the following supplemental material online at http://links.lww.com/JSN/E684.

Supplemental Table 1. RT-qPCR primer sequences.

Supplemental Table 2. The sequencing and mapping statistics of bulk RNA-seq.

Supplemental Table 3. The sequencing and mapping statistics of single-nuclear RNA-seq.

Supplemental Table 4. Glomerular bulk RNA-seq gene-set enrichment analysis results of KEGG pathways comparing Tg26 with WT.

Supplemental Table 5. Glomerular bulk RNA-seq gene-set enrichment analysis results of KEGG pathways comparing G1xTg26 with G0xTg26.

Supplemental Table 6. Glomerular bulk RNA-seq gene-set enrichment analysis results of KEGG pathways comparing G0xTg26 with Tg26.

Supplemental Figure 1. Representative images of ISH and IHC of APOL1.

Supplemental Figure 2. Bulk RNA-seq of BAC/APOL1xTg26 dual transgenic HIVAN mouse kidney.

Supplemental Figure 3. Single-nucleus RNA-seq: additional results.

Supplemental Figure 4. Gene-set enrichment analysis results of glomerular bulk RNA-seq data using podocyte DEG sets from snRNA-seq.

Supplemental Figure 5. Gene-set enrichment analysis results of glomerular bulk RNA-seq data using endothelial cell DEG sets from snRNA-seq.

Supplemental Figure 6. Gene-set enrichment analysis results of human FSGS glomerular RNA-seq data using endothelial cell DEG sets from snRNA-seq.

Supplemental Figure 7. Additional cell–cell interaction analysis results from snRNA-seq.

Supplemental Figure 8. Mouse genetic background analysis results by the MiniMUGA Assay.

References

1. Genovese G, Friedman DJ, Ross MD, et al. Association of trypanolytic ApoL1 variants with kidney disease in African Americans. *Science.* 2010;329(5993):841–845. doi:10.1126/science.1193032
2. Tzur S, Rosset S, Shemer R, et al. Missense mutations in the APOL1 gene are highly associated with end stage kidney disease risk previously attributed to the MYH9 gene. *Hum Genet.* 2010;128(3):345–350. doi:10.1007/s00439-010-0861-0
3. Daneshpajouhnejad P, Kopp JB, Winkler CA, Rosenberg AZ. The evolving story of apolipoprotein L1 nephropathy: the end of the beginning. *Nat Rev Nephrol.* 2022;18(5):307–320. doi:10.1038/s41581-022-00538-3
4. Reidy KJ, Hjorten R, Parekh RS. Genetic risk of APOL1 and kidney disease in children and young adults of African ancestry. *Curr Opin Pediatr.* 2018;30(2):252–259. doi:10.1097/MOP.0000000000000603
5. Kopp JB, Winkler CA. Genetic testing for APOL1 genetic variants in clinical practice: finally starting to arrive. *Clin J Am Soc Nephrol.* 2020;15(1):126–128. doi:10.2215/CJN.01810219
6. Freedman BI, Larsen CP. Apolipoprotein L1 gene testing comes of age. *Kidney360.* 2020;1(1):58–61. doi:10.34067/kid.0000162019
7. Egbuna O, Zimmerman B, Manos G, et al. Inaxaplin for proteinuric kidney disease in persons with two APOL1 variants. *N Engl J Med.* 2023;388(11):969–979. doi:10.1056/NEJMoa2202396
8. Yoshida T, Latt KZ, Heymann J, Kopp JB. Lessons from APOL1 animal models. *Front Med (Lausanne).* 2021;8:762901. doi:10.3389/fmed.2021.762901
9. Beckerman P, Bi-Karchin J, Park AS, et al. Transgenic expression of human APOL1 risk variants in podocytes induces kidney disease in mice. *Nat Med.* 2017;23(4):429–438. doi:10.1038/nm.4287
10. Wu J, Raman A, Coffey NJ, et al. The key role of NLRP3 and STING in APOL1-associated podocytopathy. *J Clin Invest.* 2021;131(20):e136329. doi:10.1172/jci136329
11. Ge M, Molina J, Ducasa GM, et al. APOL1 risk variants affect podocyte lipid homeostasis and energy production in focal segmental glomerulosclerosis. *Hum Mol Genet.* 2021;30(3-4):182–197. doi:10.1093/hmg/ddab022
12. McCarthy GM, Blasio A, Donovan OG, et al. Recessive, gain-of-function toxicity in an APOL1 BAC transgenic mouse model mirrors human APOL1 kidney disease. *Dis Model Mech.* 2021;14(8):dmm048952. doi:10.1242/dmm.048952
13. Ryu JH, Ge M, Merscher S, et al. APOL1 renal risk variants promote cholesterol accumulation in tissues and cultured macrophages from APOL1 transgenic mice. *PLoS One.* 2019;14(4):e0211559. doi:10.1371/journal.pone.0211559
14. Okamoto K, Rausch JW, Wakashin H, et al. APOL1 risk allele RNA contributes to renal toxicity by activating protein kinase R. *Commun Biol.* 2018;1:188. doi:10.1038/s42003-018-0188-2
15. Blessing NA, Wu Z, Madhavan SM, et al. Lack of APOL1 in proximal tubules of normal human kidneys and proteinuric APOL1 transgenic mouse kidneys. *PLoS One.* 2021;16(6):e0253197. doi:10.1371/journal.pone.0253197
16. Aghajan M, Booten SL, Althage M, et al. Antisense oligonucleotide treatment ameliorates IFN-γ-induced proteinuria in APOL1-transgenic mice. *JCI Insight.* 2019;4(12):e126124. doi:10.1172/jci.insight.126124
17. Kopp JB, Nelson GW, Sampath K, et al. APOL1 genetic variants in focal segmental glomerulosclerosis and HIV-associated nephropathy. *J Am Soc Nephrol.* 2011;22(11):2129–2137. doi:10.1681/ASN.2011040388
18. Kasembeli AN, Duarte R, Ramsay M, et al. APOL1 risk variants are strongly associated with HIV-associated nephropathy in Black South Africans. *J Am Soc Nephrol.* 2015;26(11):2882–2890. doi:10.1681/ASN.2014050469
19. Dickie P, Felser J, Eckhaus M, et al. HIV-associated nephropathy in transgenic mice expressing HIV-1 genes. *Virology.* 1991;185(1):109–119. doi:10.1016/0042-6822(91)90759-5
20. Kopp JB, Klotman ME, Adler SH, et al. Progressive glomerulosclerosis and enhanced renal accumulation of basement membrane components in mice transgenic for human immunodeficiency virus type 1 genes. *Proc Natl Acad Sci U S A.* 1992;89(5):1577–1581. doi:10.1073/pnas.89.5.1577
21. Lannon H, Shah SS, Dias L, et al. Apolipoprotein L1 (APOL1) risk variant toxicity depends on the haplotype background. *Kidney Int.* 2019;96(6):1303–1307. doi:10.1016/j.kint.2019.07.010
22. Scales SJ, Gupta N, De Mazière AM, et al. Apolipoprotein L1-specific antibodies detect endogenous APOL1 inside the endoplasmic reticulum and on the plasma membrane of podocytes. *J Am Soc Nephrol.* 2020;31(9):2044–2064. doi:10.1681/ASN.2019080829
23. Santo BA, Govind D, Daneshpajouhnejad P, et al. PodoCount: a robust, fully automated, whole-slide podocyte quantification tool. *Kidney Int Rep.* 2022;7(6):1377–1392. doi:10.1016/j.ekir.2022.03.004
24. Lutnick B, Ginley B, Govind D, et al. An integrated iterative annotation technique for easing neural network training in medical image analysis. *Nat Mach Intell.* 2019;1(2):112–119. doi:10.1038/s42256-019-0018-3
25. Kikuchi M, Wickman L, Hodgin JB, Wiggins RC. Podometrics as a potential clinical tool for glomerular disease management. *Semin Nephrol.* 2015;35(3):245–255. doi:10.1016/j.semnephrol.2015.04.004
26. Venkatareddy M, Wang S, Yang Y, et al. Estimating podocyte number and density using a single histologic section. *J Am Soc Nephrol.* 2014;25(5):1118–1129. doi:10.1681/ASN.2013080859
27. Love MI, Huber W, Anders S. Moderated estimation of fold change and dispersion for RNA-seq data with DESeq2. *Genome Biol.* 2014;15(12):550. doi:10.1186/s13059-014-0550-8
28. Subramanian A, Tamayo P, Mootha VK, et al. Gene set enrichment analysis: a knowledge-based approach for interpreting genome-wide expression profiles. *Proc Natl Acad Sci U S A.* 2005;102(43):15545–15550. doi:10.1073/pnas.0506580102
29. Mootha VK, Lindgren CM, Eriksson KF, et al. PGC-1alpha-responsive genes involved in oxidative phosphorylation are coordinately downregulated in human diabetes. *Nat Genet.* 2003;34(3):267–273. doi:10.1038/ng1180
30. Langfelder P, Horvath S. WGCNA: an R package for weighted correlation network analysis. *BMC Bioinformatics.* 2008;9(1):559. doi:10.1186/1471-2105-9-559
31. Zhou G, Soufan O, Ewald J, Hancock REW, Basu N, Xia J. NetworkAnalyst 3.0: a visual analytics platform for comprehensive gene expression profiling and meta-analysis. *Nucleic Acids Res.* 2019;47(W1):W234–W241. doi:10.1093/nar/gkz240
32. Kirita Y, Wu H, Uchimura K, Wilson PC, Humphreys BD. Cell profiling of mouse acute kidney injury reveals conserved cellular responses to injury. *Proc Natl Acad Sci U S A.* 2020;117(27):15874–15883. doi:10.1073/pnas.2005477117
33. Young MD, Behjati S. SoupX removes ambient RNA contamination from droplet-based single-cell RNA sequencing data. *GigaScience.* 2020;9(12):giaa151. doi:10.1093/gigascience/giaa151

34. Hao Y, Hao S, Andersen-Nissen E, et al. Integrated analysis of multimodal single-cell data. *Cell.* 2021;184(13):3573–3587.e29. doi:10.1016/j.cell.2021.04.048
35. Kramer A, Green J, Pollard J Jr., Tugendreich S. Causal analysis approaches in ingenuity pathway analysis. *Bioinformatics.* 2014;30(4):523–530. doi:10.1093/bioinformatics/btt703
36. Jin S, Guerrero-Juarez CF, Zhang L, et al. Inference and analysis of cell-cell communication using CellChat. *Nat Commun.* 2021;12(1):1088. doi:10.1038/s41467-021-21246-9
37. McNulty MT, Fermin D, Eichinger F, et al. A glomerular transcriptomic landscape of apolipoprotein L1 in Black patients with focal segmental glomerulosclerosis. *Kidney Int.* 2022;102(1):136–148. doi:10.1016/j.kint.2021.10.041
38. Gadegbeku CA, Gipson DS, Holzman LB, et al. Design of the Nephrotic Syndrome Study Network (NEPTUNE) to evaluate primary glomerular nephropathy by a multidisciplinary approach. *Kidney Int.* 2013;83(4):749–756. doi:10.1038/ki.2012.428
39. Latt KZ, Heymann J, Jessee JH, et al. Urine single-cell RNA sequencing in focal segmental glomerulosclerosis reveals inflammatory signatures. *Kidney Int Rep.* 2022;7(2):289–304. doi:10.1016/j.ekir.2021.11.005
40. Yoshida T, Latt KZ, Rosenberg AZ, et al. Transcriptomic analysis of human podocytes in vitro: effects of differentiation and APOL1 genotype. *Kidney Int Rep.* 2023;8(1):164–178. doi:10.1016/j.ekir.2022.10.011
41. Lefebvre J, Clarkson M, Massa F, et al. Alternatively spliced isoforms of WT1 control podocyte-specific gene expression. *Kidney Int.* 2015;88(2):321–331. doi:10.1038/ki.2015.140
42. Puelles VG, van der Wolde JW, Wanner N, et al. mTOR-mediated podocyte hypertrophy regulates glomerular integrity in mice and humans. *JCI Insight.* 2019;4(18):e99271. doi:10.1172/jci.insight.99271
43. Jaworski A, Tom I, Tong RK, et al. Operational redundancy in axon guidance through the multifunctional receptor Robo3 and its ligand NELL2. *Science.* 2015;350(6263):961–965. doi:10.1126/science.aad2615
44. Pak JS, DeLoughery ZJ, Wang J, et al. NELL2-Robo3 complex structure reveals mechanisms of receptor activation for axon guidance. *Nat Commun.* 2020;11(1):1489. doi:10.1038/s41467-020-15211-1
45. Faherty N, O'Donovan H, Kavanagh D, et al. TGFβ and CCN2/CTGF mediate actin related gene expression by differential E2F1/CREB activation. *BMC Genomics.* 2013;14:525. doi:10.1186/1471-2164-14-525
46. Phanish MK, Winn SK, Dockrell ME. Connective tissue growth factor-(CTGF, CCN2)–a marker, mediator and therapeutic target for renal fibrosis. *Nephron Exp Nephrol.* 2010;114(3):e83–e92. doi:10.1159/000262316
47. Lee YC, Kaufmann M, Kitazume-Kawaguchi S, et al. Molecular cloning and functional expression of two members of mouse NeuAcalpha2,3Galbeta1,3GalNAc GalNAcalpha2,6-sialyltransferase family, ST6GalNAc III and IV. *J Biol Chem.* 1999;274(17):11958–11967. doi:10.1074/jbc.274.17.11958
48. Niculovic KM, Blume L, Wedekind H, et al. Podocyte-specific sialylation-deficient mice serve as a model for human FSGS. *J Am Soc Nephrol.* 2019;30(6):1021–1035. doi:10.1681/ASN.2018090951
49. Huizing M, Yardeni T, Fuentes F, et al. Rationale and design for a phase 1 study of N-acetylmannosamine for primary glomerular diseases. *Kidney Int Rep.* 2019;4(10):1454–1462. doi:10.1016/j.ekir.2019.06.012
50. Sugo S, Minamino N, Kangawa K, et al. Endothelial cells actively synthesize and secrete adrenomedullin. *Biochem Biophys Res Commun.* 1994;201(3):1160–1166. doi:10.1006/bbrc.1994.1827
51. Ichiki Y, Kitamura K, Kangawa K, Kawamoto M, Matsuo H, Eto T. Distribution and characterization of immunoreactive adrenomedullin in human tissue and plasma. *FEBS Lett.* 1994;338(1):6–10. doi:10.1016/0014-5793(94)80106-1
52. Hino M, Nagase M, Kaname S, et al. Expression and regulation of adrenomedullin in renal glomerular podocytes. *Biochem Biophys Res Commun.* 2005;330(1):178–185. doi:10.1016/j.bbrc.2005.02.142
53. Oba S, Hino M, Fujita T. Adrenomedullin protects against oxidative stress-induced podocyte injury as an endogenous antioxidant. *Nephrol Dial Transplant.* 2008;23(2):510–517. doi:10.1093/ndt/gfm600
54. Takemon Y, Chick JM, Gerdes Gyuricza I, et al. Proteomic and transcriptomic profiling reveal different aspects of aging in the kidney. *Elife.* 2021;10:e62585. doi:10.7554/eLife.62585
55. Jarad G, Pippin JW, Shankland SJ, Kreidberg JA, Miner JH. Dystroglycan does not contribute significantly to kidney development or function, in health or after injury. *Am J Physiol Renal Physiol.* 2011;300(3):F811–F820. doi:10.1152/ajprenal.00725.2010
56. Coers W, Brouwer E, Vos JT, et al. Podocyte expression of MHC class I and II and intercellular adhesion molecule-1 (ICAM-1) in experimental pauci-immune crescentic glomerulonephritis. *Clin Exp Immunol.* 1994;98(2):279–286. doi:10.1111/j.1365-2249.1994.tb06138.x
57. Piguet V, Schwartz O, Le Gall S, Trono D. The downregulation of CD4 and MHC-I by primate lentiviruses: a paradigm for the modulation of cell surface receptors. *Immunol Rev.* 1999;168:51–63. doi:10.1111/j.1600-065x.1999.tb01282.x
58. Wang H, Duan A, Zhang J, et al. Glucocorticoid receptor wields chromatin interactions to tune transcription for cytoskeleton stabilization in podocytes. *Commun Biol.* 2021;4(1):675. doi:10.1038/s42003-021-02209-8
59. Gharavi AG, Ahmad T, Wong RD, et al. Mapping a locus for susceptibility to HIV-1-associated nephropathy to mouse chromosome 3. *Proc Natl Acad Sci U S A.* 2004;101(8):2488–2493. doi:10.1073/pnas.0308649100
60. Bruggeman LA, Wu Z, Luo L, et al. APOL1-G0 protects podocytes in a mouse model of HIV-associated nephropathy. *PLoS One.* 2019;14(10):e0224408. doi:10.1371/journal.pone.0224408
61. Wakashin H, Heymann J, Roshanravan H, et al. APOL1 renal risk variants exacerbate podocyte injury by increasing inflammatory stress. *BMC Nephrol.* 2020;21(1):371. doi:10.1186/s12882-020-01995-3
62. Nichols B, Jog P, Lee JH, et al. Innate immunity pathways regulate the nephropathy gene Apolipoprotein L1. *Kidney Int.* 2015;87(2):332–342. doi:10.1038/ki.2014.270
63. Fantus D, Rogers NM, Grahammer F, Huber TB, Thomson AW. Roles of mTOR complexes in the kidney: implications for renal disease and transplantation. *Nat Rev Nephrol.* 2016;12(10):587–609. doi:10.1038/nrneph.2016.108
64. Huang Z, Liu S, Tang A, et al. Key role for EphB2 receptor in kidney fibrosis. *Clin Sci (Lond).* 2021;135(17):2127–2142. doi:10.1042/CS20210644
65. Wang Y, Nakayama M, Pitulescu ME, et al. Ephrin-B2 controls VEGF-induced angiogenesis and lymphangiogenesis. *Nature.* 2010;465(7297):483–486. doi:10.1038/nature09002
66. Gribouval O, Boyer O, Knebelmann B, et al. APOL1 risk genotype in European steroid-resistant nephrotic syndrome and/or focal segmental glomerulosclerosis patients of different African ancestries. *Nephrol Dial Transplant.* 2019;34(11):1885–1893. doi:10.1093/ndt/gfy176
67. Watanabe A, Guaragna MS, Belangero VMS, et al. APOL1 in an ethnically diverse pediatric population with nephrotic syndrome: implications in focal segmental glomerulosclerosis and other diagnoses. *Pediatr Nephrol.* 2021;36(8):2327–2336. doi:10.1007/s00467-021-04960-w